

~~RESTRICTED~~ UNCLASSIFIED

Copy

6

RM A50A13

C. 2

NACA

RESEARCH MEMORANDUM

AN EXPERIMENTAL INVESTIGATION OF A JET-ENGINE NACELLE
IN SEVERAL POSITIONS ON A 37.25° SWEPT-BACK WING

By Robert E. Dannenberg and James R. Blackaby

Ames Aeronautical Laboratory
Moffett Field, Calif.

CLASSIFICATION CANCELLED

Authority J. W. Crowley Date 12/4/53
EO 10501
By INTA 1/6/54 See None
CLASSIFIED DOCUMENT R7 1843

This document contains classified information affecting the National Defense of the United States within the meaning of the Espionage Act, USC 8031 and 32. Its transmission or the revelation of its contents in any manner to an unauthorized person is prohibited by law. Information so classified may be imparted only to persons in the military and naval services of the United States, appropriate civilian officers and employees of the Federal Government who have a legitimate interest therein, and to United States citizens of known loyalty and discretion who of necessity must be informed thereof.

NATIONAL ADVISORY COMMITTEE
FOR AERONAUTICS

WASHINGTON

April 19, 1950

~~RESTRICTED~~

UNCLASSIFIED



UNCLASSIFIED

NATIONAL ADVISORY COMMITTEE FOR AERONAUTICS

RESEARCH MEMORANDUM

AN EXPERIMENTAL INVESTIGATION OF A JET-ENGINE NACELLE

IN SEVERAL POSITIONS ON A 37.25° SWEPT-BACK WING

By Robert E. Dannenberg and James R. Blackaby

SUMMARY

Wind-tunnel tests of a jet-engine nacelle on a semispan wing having the leading edge swept back 37.25° were made to determine the effects of the nacelle on the aerodynamic characteristics of the wing. The wing had an aspect ratio of 6.04 and the tip chord was half the root chord. The nacelle was mounted in three positions: centrally and low on the wing at the 31-percent-semispan station and centrally at the wing tip.

In comparison with the force characteristics of the wing alone, the addition of the nacelle to the wing in each position resulted in favorable interference on the maximum-lift and pitching-moment characteristics and in a small increase in drag.

The ram-pressure recovery in the inlets was at least 95 percent of free-stream ram pressure for inlet-velocity ratios less than unity and positive angles of attack up to 7° .

For the wing-nacelle combinations, the critical Mach numbers predicted for locations corresponding to the crest of the airfoil did not vary with inlet velocity and were, in general, higher than those predicted for the crest of the airfoil alone. The crest was defined as the location at which the airfoil surface was tangent to the free-stream direction.

INTRODUCTION

Tests were reported in reference 1 of the effects on the low-speed aerodynamic characteristics of a wing with the leading edge swept back 37.25° produced by the addition of a nacelle in various positions on the wing. That nacelle was a solid ellipsoidal body with a fineness ratio of 5.0 and it had no provision for internal air flow. The present report is a continuation of the investigation reported in reference 1 and presents a summation of the effects accompanying the addition of a nacelle with internal air flow to the same swept-back wing. The nacelle was mounted at the 31-percent-semispan station of the wing in a central and in an underslung position and also at the wing tip in a central position.



UNCLASSIFIED

In accordance with the findings of reference 1, the leading edge of the nacelle for each nacelle position was located at or near the leading edge of the wing in an attempt to obtain favorable velocity distributions in the wing-nacelle junctures. Two air inlets, one normal to the nacelle axis and one swept nearly parallel to the leading edge of the wing, were tested on the nacelle in the underslung inboard position. The nacelle in the central inboard position had a swept air inlet at the leading edge of the wing, while in the tip position the nacelle had an air inlet normal to the longitudinal axis.

Force and pressure-distribution measurements were obtained for the wing alone and for the wing with the nacelle in each of the three positions.

NOTATION

The following coefficients and symbols are used:

$b/2$	wing semispan normal to root chord, feet
c	local wing chord parallel to root chord, feet
\bar{c}	mean aerodynamic chord $\left(\frac{\int_0^{b/2} c^2 dy}{\int_0^{b/2} c dy} \right)$, feet
C_D	drag coefficient $(D/q_0 S)$
C_{D_F}	drag coefficient of nacelle (excluding internal drag) based on nacelle frontal area $(\Delta D/q_0 F)$
C_L	lift coefficient $(L/q_0 S)$
C_m	pitching-moment coefficient $(M/q_0 S \bar{c})$
D	drag, pounds
ΔD	external drag increment due to nacelle, pounds
d	basic nacelle inlet diameter, inches
F	nacelle frontal area, square feet
H	total pressure, pounds per square foot

$\frac{H_2 - P_0}{H_0 - P_0}$	ram-recovery ratio
L	lift, pounds
M	pitching moment about a lateral axis through the quarter point of the mean aerodynamic chord, foot-pounds
P	pressure coefficient $\left(\frac{P_l - P_0}{q_0} \right)$
p	static pressure, pounds per square foot
q	dynamic pressure, pounds per square foot $\left(\frac{1}{2} \rho V^2 \right)$
S	wing area (semispan), square feet
t	maximum nacelle diameter, inches
V	velocity, feet per second
V_1/V_0	inlet-velocity ratio
X	basic nacelle forebody length, inches
y	perpendicular distance from root chord along semispan, feet
α	angle of attack, degrees
ρ	mass density, slugs per cubic foot

Subscripts

l	local
o	free stream
u	uncorrected
1	station of minimum inlet area
2	station of inlet rake

MODEL AND APPARATUS

The model wing, of 5-foot semispan, used for these tests had the leading edge swept back 37.25° , the aspect ratio was 6.04 based on full

span, and the ratio of tip chord to root chord was 0.5. Normal to the 27.06-percent-chord line (measured streamwise), the wing had the NACA 64₁-212 section and there was no twist. A sketch of the plan form of the wing is shown in figure 1. Coordinates for the NACA 64₁-212 airfoil section are given in reference 2. Coordinates for sections parallel to the direction of the free stream are presented in table I.

The semispan wing was mounted in one of the Ames 7- by 10-foot wind tunnels on a dummy tunnel floor which served as a reflection plane simulating a plane of symmetry (fig. 2). The dummy floor, which separated the boundary layer of the tunnel floor from the model, extended 8 feet upstream and 9 feet downstream from the center of rotation of the model. A fairing was provided around the portion of the model between the turntables of the tunnel floor and of the dummy floor. There was a gap of approximately 1/8 inch between the end of the model and the turntable of the dummy floor to permit the forces acting on only the model to be measured by the tunnel balance system. This gap was made small to keep air leakage into the tunnel near the model to a minimum.

The nacelle was mounted on the wing in both a central and an underslung position at the 31-percent-semispan station and in a central position at the wing tip. (See fig. 3.) In the central position, the nacelle axis was coincident with the wing chord plane. In the underslung position, the nacelle axis was 1.25 inches below the wing chord plane. Pertinent details of the nacelle are given in table II.

DESIGN OF NACELLE

The nacelle design was dictated by the size and air requirements of a jet engine 39 inches in diameter. The model scale was selected as one-sixth full scale for the nacelle in the inboard positions. This was thought to be too large for a nacelle at the wing tip so, for the tip position, the scale was reduced to one-seventh full scale. The basic nacelle shape was an axially symmetric body based on parameters introduced in the development of the NACA 1-series nose inlets in reference 3. These parameters include the ratios of inlet diameter and forebody length to maximum nacelle diameter.

The maximum nacelle diameter, governed by the jet-engine diameter plus an allowance for structural members, was 7.20 inches, model scale. A fineness ratio of 5, based on the actual basic nacelle-body length, was chosen since that value was used in the preliminary solid-body investigation (reference 1). The resulting basic nacelle length was 36 inches. This was equal to about 1.6 times the wing chord at the inboard nacelle station and was considered to be in keeping with current high-speed design practice.

The ratio of inlet diameter to maximum nacelle diameter (d/t) was selected as 0.45 in order to satisfy the engine air requirements for an inlet-velocity ratio of 0.55, corresponding to a true airspeed of 550 miles per hour at an altitude of 40,000 feet. The NACA 1-series design charts (reference 3) were entered with these design parameters:

$$d/t = 0.45$$

$$V_1/V_0 = 0.55$$

and the ratio of nacelle forebody length to maximum diameter was selected as

$$X/t = 2.0$$

yielding a forebody length of 14.4 inches. With these values for the design parameters, the charts indicated that velocity peaks would not form over the lips of the isolated nacelle operating with the design inlet-velocity ratio.

For the external forebody shape, the NACA 1-series profile was closely approximated by a second-degree curve constructed by the method of conic lofting described in reference 4. The NACA 1-series shape at the nose was replaced by an arc with a radius of 0.1513 inches. The shape of the nacelle afterbody was designed to avoid severe pressure gradients and was tapered and then cusped near the outlet.

A nacelle of this basic design would not ordinarily be mounted inboard on the swept wing with its nose at the leading edge of the wing without modifications to the inlet. With the nacelle in the central position on the wing at 31 percent of the semispan, the inlet was swept to coincide with the wing leading edge (figs. 3(a) and 4). This sweeping was accomplished by translating the lofting control lines of the basic forebody shape fore or aft so that the plane of the nacelle leading edge corresponded to a plane at the wing leading edge perpendicular to the wing-chord plane.

Further modification of the inlet was necessary for the nacelle in the underslung position. In order to avoid acute angles between the nacelle and the wing near the wing leading edge, and, at the same time to keep the position of maximum thickness relative to the wing chord the same as for the nacelle in the central position on the wing, the forebody length of the basic design was reduced. Thus, at 31 percent of the semispan of the wing, the plane of the nacelle entrance was located at the 10-percent-chord station. The nacelle entrance was normal to the air stream (figs. 3(b) and 5). To avoid extensive filleting of the lower surface of the wing-nacelle junctures, the upper portion of the basic nacelle was allowed to extend above the upper surface of the wing (fig. 2(b)), and the cross section of the nacelle forebody between the nacelle reference plane (fig. 5) and the lower surface of the wing was altered slightly so the nacelle surface would intersect the lower surface of the wing nearly at right angles. With the nacelle in this

position, the jet engine would extend through the wing but probably would not interfere with the front wing spar.

For a modification of the underslung design, the forebody elements were translated fore or aft so that the plane of the air inlet of the nacelle was swept along a line at 10 percent of the wing chord measured in the streamwise direction (figs. 3(c) and 6).

For the nacelle at the wing tip, the size was reduced to one-seventh full scale while the design shape was maintained. The inlet was placed at the wing leading edge. (See figs. 3(d) and 7.)

No attempt was made to design proper internal ducting downstream of the inlet rakes. (See figs. 4 through 7.) The basic design, exemplified in the central inboard and tip positions, included a simulated jet-engine accessory housing. However, in the underslung positions, an asymmetric duct was employed as shown in figures 5 and 6.

TESTS

Measurements of lift, drag, pitching moment, ram-pressure recovery, and surface pressures at various angles of attack were made at a test Mach number of 0.16 and a Reynolds number of 1,880,000 based on the mean aerodynamic chord of the wing. In addition, drag data for the model at an angle of attack of zero and an inlet-velocity ratio of zero were obtained for various test Mach numbers up to 0.33, and a Reynolds number of 3,700,000. Tunnel-wall corrections to the force measurements were applied according to the methods discussed in reference 5, with modifications to account for the effects of sweepback:

$$\alpha = \alpha_u + 0.985 C_{L_u}$$

$$C_D = C_{D_u} + 0.020 C_{L_u}^2$$

The effects of the boundary layer of the dummy floor and of air leakage between the wing root and the floor plates on the characteristics of the model were not determined. These effects are believed to have been small.

Force measurements and pressure-distribution data were obtained separately. During force measurements, the internal air flow was regulated by changing screens in the nacelle duct behind the entrance rake. Figure 8 shows the variation of inlet-velocity ratio with angle of attack with screens providing nominal inlet-velocity ratios of 0.3 and 0.6 and with the screens removed to permit maximum flow. Force and pressure studies for an inlet-velocity ratio of zero were made with a flush plug and with a faired plug in the tail pipe as shown in figure 9.

During pressure-distribution measurements, air flow through the nacelle was maintained by a variable-speed centrifugal compressor outside the wind-tunnel test chamber. A flexible rubber hose, fastened to the nacelle tail pipe, was used to connect the nacelle to the suction system. The quantity of internal air flow was measured by a calibrated orifice meter.

The duct-entrance losses were measured by rakes of total- and static-pressure tubes. The rake locations are shown in figures 4 to 7. The pressure distribution over the upper- and lower-surface center lines of the nacelle and in the wing-nacelle junctures was measured by flush orifices connected to multiple-tube manometers. The manometer readings were recorded photographically. Tuft studies of the flow over the upper surface of the model were made with the nacelle in each position. In conjunction with the force measurements, the total-pressure losses through the nacelle duct were measured by means of a rake of pressure tubes mounted independently of the model at the tail-pipe exit as shown in figure 10. The pressure-loss data were then utilized to compute the internal drag of the nacelle for each position. The external drag due to the addition of the nacelle to the wing was obtained by subtracting the drag of the plain wing and the internal drag from the total model drag as measured by the scale system. Since the external drag of the nacelle was small compared to the total drag of the model, there was considerable scatter in the external nacelle drag results.

RESULTS AND DISCUSSION

Force Characteristics

Plain wing.— The lift and pitching-moment coefficients of the plain wing are shown in figure 11 for the test Reynolds number of 1,880,000. In addition, the force characteristics of the same wing for a test Reynolds number of 2,700,000, obtained from reference 1, are presented. Inspection of the figure indicates that in comparison with the results of reference 1, the data from the present test, at the lower Reynolds number, show some reduction in the lift-curve slope at the higher angles of attack and a reduction of the lift coefficient at which the pitching moment became unstable.

Wing with nacelle.— The lift and stability characteristics of the wing with the nacelle in the various positions are given in figures 12 through 15, and some of the characteristics are summarized in table III. A study of these data reveals that the nacelle in its various positions produced only small effects on the lift and on the static longitudinal stability of the wing. The slope of the lift curve of the wing was only slightly affected by the nacelle in the inboard positions, but was increased somewhat by the nacelle in the tip position. In all the positions, the nacelle delayed the unstable break in pitching moment to lift coefficients slightly higher than for the wing alone. At lift coefficients beyond the beginning of the stall, all the configurations were unstable. Up to the highest test angle of attack, 20° , maximum lift had not been reached for the wing or for any of the wing-nacelle combinations. The lift and stability characteristics were found to be practically independent of inlet-velocity ratio.

The total-drag polars are presented in figure 16 for the wing and for the wing with the nacelle in the various positions with a faired tail-pipe plug to provide an inlet-velocity ratio of zero. The variation of the nacelle drag coefficient in the different positions, based on the nacelle frontal area, is shown in figure 17 for inlet-velocity ratios of zero and 0.6. The data show that, for an inlet-velocity ratio of 0.6, nacelle position had but little effect on the variation of the external drag coefficient with lift coefficient. Values of nacelle drag coefficient are presented in table III.

For zero inlet velocity, the effect of a flush tail-pipe plug was investigated. In comparison with the faired tail-pipe characteristics, the only appreciable effect attributable to the flush plug was an increment of drag coefficient. For the nacelle in the central inboard position, a representative case, the following increments in drag coefficient (based on wing area) were observed:

C_L	C_D Increment
-0.1	0.0007
0	.0009
.15	.0009
.30	.0005

For lift coefficients greater than 0.35, the drag-coefficient increment was 0.0002 or less.

The variation of drag coefficient with Reynolds number for the wing and for the wing with the nacelle in the various positions is presented in figure 18 for an angle of attack of 0° and an inlet velocity of zero. It is shown that the addition of the nacelle to the wing in any one of the positions caused a drag increment which was relatively constant throughout the range of Reynolds numbers investigated.

Internal Pressure Recovery

The variation of ram-pressure recovery inside the entrance of the nacelle is shown in figures 12 to 15. For inlet-velocity ratios greater than zero and less than unity, at least 95 percent of the free-stream ram pressure was recovered in the nacelle for positive angles of attack up to 7° for the nacelle in each position. The best recovery characteristics were obtained with the nacelle in the underslung inboard position with the

inlet normal to the air stream (fig. 13). The effect of inlet-velocity ratio on the ram-pressure recovery was small, except with the nacelle in the central inboard position (fig. 12). The increase in the entrance losses at the higher angles of attack was found to result from stalled flow on the inner surface of the inboard portion of the duct lip.

External Pressure Distribution

The pressure distribution over the center lines of the upper and lower surfaces of the nacelle and in the wing-nacelle junctures for the nacelle in each position is presented in the following figures for inlet-velocity ratios of 0 and 0.6:

Nacelle position	Center lines		Inboard junctures		Outboard junctures	
	Upper surface	Lower surface	Upper	Lower	Upper	Lower
Central inboard	19(a)	19(b)	19(c)	19(d)	19(e)	19(f)
Underslung inboard with normal inlet	20(a)	20(b)	20(c)	20(d)	20(e)	20(f)
Underslung inboard with swept inlet	-	21(a)	-	21(b)	-	21(c)
Tip	22(a)	22(b)	22(c)	22(d)	22(e)	

The upper-surface pressure distribution for the nacelle in the underslung inboard position with the swept inlet is not presented since, for all practical purposes, it was the same as that for the nacelle in the same position with the normal inlet.

The pressure distribution over the nacelle in each position shows the existence of localized regions near the duct entrance over which the velocities were in excess of the maximum velocities over the plain wing at 31-percent semispan (fig. 11). However, behind approximately 5 percent of the nacelle length, the velocities over the nacelle were less than those over the plain wing at 31-percent semispan. The saddle in the pressure distribution on the upper surface between 5 and 10 percent of the nacelle length for the nacelle in the underslung inboard position (fig. 20(a)) was due to the nacelle extending above the wing as shown in figures 2(b) and 5. An increased velocity was noted over the afterbody of the nacelle in the tip position as shown in figure 22(a).

Studies of the pressure distribution over the nacelle in the various positions on the wing were made with inlet-velocity ratios of 0, 0.3, 0.6, 0.9, and 1.2. Only the results for inlet-velocity ratios of 0 and 0.6 are presented. The major effect of increasing inlet-velocity ratio was a decrease in the velocities over the leading 15 percent of the nacelle length. Behind about 15 percent of the nacelle length, or 20 percent of the wing chord in the junctures, the pressure distribution was affected only slightly by inlet-velocity changes.

Critical Mach Number

The variations of the predicted minimum critical Mach number with angle of attack for the upper surface of the nacelle and in the wing-nacelle junctures for all the test inlet-velocity ratios are shown in figure 23. The critical Mach numbers for these curves were predicted from the test values of the minimum pressure coefficients for each test condition by the application of the Karman-Tsien hodograph method as discussed in reference 6; no correction was applied for the effects of sweepback.

In table IV, values of critical Mach number are tabulated for the range of low-speed pressure coefficients obtained in the present test. The data of figure 23 and table IV can be used to determine the minimum low-speed pressure coefficient for any angle of attack and inlet velocity ratio. The minimum pressure coefficient can then be utilized in interpolating or extrapolating between or beyond the pressure-distribution curves presented for inlet velocity ratios of 0 and 0.6 in figures 19 through 22.

From analyses of experimental high-speed data, references 7 and 8 have shown that the Mach number for which sonic velocity occurs at the crest of an airfoil (the chordwise station at which the upper surface of the airfoil is tangent to the free-stream direction) may be a better estimation of the Mach number for which the abrupt supercritical drag rise begins than is the Mach number associated with the initial occurrence of sonic velocity on the airfoil. A similar conclusion was reported in reference 9 from high-speed tests of the wing of the present investigation.

In order to indicate an equitable evaluation of the effect of the nacelle of the present test on the Mach number associated with the abrupt supercritical drag rise of the wing at high speed, local (or sectional) values of both the minimum critical Mach numbers and the critical Mach numbers at the airfoil crest have been predicted. They have been predicted by utilizing the Karman-Tsien method (table IV) to extrapolate the low-speed pressure coefficients to values associated with the occurrence of local sonic velocities. The effects of sweep on the critical pressure coefficient, as discussed in reference 9, were not included in the calculations since insufficient data were obtained to permit a determination of

the isobars on the wing and nacelle combination. The variations of the minimum critical Mach number and of the critical Mach number at the crest with angle of attack for the wing at 31 percent of the semispan are shown in figure 11. Corresponding curves for the wing with the nacelle in the various positions are shown in figures 19 through 22. A comparison of the data indicates that the critical Mach numbers predicted from pressure coefficients for the wing-nacelle combinations at stations corresponding to the crest of the airfoil are, in general, higher than those predicted for the plain wing. Therefore, it appears that the addition of the nacelle to the wing in the various positions would cause no decrease in the free-stream Mach number at which the abrupt drag rise would begin in high-speed flight. In addition, a study of the critical Mach numbers at stations corresponding to the airfoil crest indicates that the effect of varying inlet-velocity ratio should have little effect on the Mach number for drag divergence.

Tuft Studies

Photographs made during tuft studies are included in figure 24 to show the flow over the upper surface of the wing with and without the nacelle. The results for only one of the underslung inboard nacelle designs are presented since the flow over the upper surface of the model was similar for the two designs. The tufts indicate that the addition of the nacelle did not greatly affect the stall pattern or the progression of the stall with increasing angle of attack.

CONCLUDING REMARKS

A nacelle with an inlet in its nose at or near the wing leading edge had little effect on the lift characteristics of a model wing with its leading edge swept back 37.25° . The drag increment due to the nacelle, based on its frontal area, was of the order of 0.045 for the nacelle at 31 percent of the semispan and 0.035 for the nacelle at the wing tip. The addition of the nacelle increased the static longitudinal stability slightly over that for the plain wing and generally increased the lift coefficient at which an unstable break in the pitching moment occurred. Changing the inlet-velocity ratio had little effect on the lift and pitching moment. Tuft studies indicated that the addition of the nacelle to the wing had little effect on the stall pattern.

Increasing the inlet-velocity ratio reduced the local velocities over the nacelle lips, thereby increasing the predicted minimum critical Mach numbers for the wing-nacelle combinations. However, the critical Mach numbers predicted for the wing-nacelle combinations for stations corresponding to the crest of the airfoil were nearly independent of

inlet-velocity ratio and they were generally higher than those predicted for the crest of the plain wing.

For positive angles of attack up to 7° , and for inlet-velocity ratios less than unity, the ram-pressure recovery inside the nacelle entrance was at least 95 percent of the free-stream ram pressure for the nacelle in each position.

National Advisory Committee for Aeronautics,
Ames Aeronautical Laboratory,
Moffett Field, Calif.

REFERENCES

1. Hanson, Frederick H., Jr., and Dannenberg, Robert E.: Effect of a Nacelle on the Low-Speed Aerodynamic Characteristics of a Swept-Back Wing. NACA RM A8E12, 1948.
2. Abbott, Ira H., von Doenhoff, Albert E., and Stivers, Louis S., Jr.: Summary of Airfoil Data. NACA Rep. 824, 1945.
3. Baals, Donald D., Smith, Norman F., and Wright, John B.: The Development and Application of High-Critical-Speed Nose Inlets. NACA ACR L5F30a, 1945.
4. Liming, Roy A.: Practical Analytic Geometry with Applications to Aircraft. The Macmillan Company, N. Y., 1944.
5. Glauert, H.: The Elements of Aerofoil and Airscrew Theory. The Macmillan Company, N. Y., 1943.
6. Liepmann, H. W., and Puckett, A. E.: Introduction to Aerodynamics of a Compressible Fluid. John Wiley & Sons, Inc., N. Y., 1947, pp. 184-186, 244-247.
7. Nitzberg, Gerald E., and Crandall, Stewart: A Study of Flow Changes Associated with Airfoil Section Drag Rise at Supercritical Speeds. NACA TN 1813, 1949.
8. Nitzberg, Gerald E., Crandall, Stewart M., and Polentz, Perry P.: A Preliminary Investigation of the Usefulness of Camber in Obtaining Favorable Airfoil-Section Drag Characteristics at Supercritical Speeds. NACA RM A9G20, 1949.
9. Edwards, George G., and Boltz, Frederick W.: An Analysis of the Forces and Pressure Distribution on a Wing with the Leading Edge Swept Back 37.25° . NACA RM A9K01, 1949.

TABLE I

COORDINATES FOR AIRFOIL
SECTIONS PARALLEL TO FREE AIR STREAM
[Stations and ordinates given in
percent of airfoil chord]

Upper Surface		Lower Surface	
Station	Ordinate	Station	Ordinate
0	0	0	0
.465	.908	.647	-.820
.733	1.103	.935	-.979
1.275	1.411	1.504	-1.221
2.644	1.961	2.905	-1.632
5.388	2.754	5.679	-2.196
8.129	3.355	8.426	-2.608
10.859	3.846	11.153	-2.939
16.279	4.614	16.555	-3.439
21.647	5.175	21.890	-3.794
26.959	5.580	27.163	-4.035
32.213	5.845	32.378	-4.177
37.413	5.978	37.534	-4.220
42.555	5.983	42.635	-4.165
47.644	5.816	47.680	-3.968
52.674	5.525	52.674	-3.673
57.649	5.135	57.618	-3.307
62.569	4.666	62.512	-2.887
67.433	4.133	67.358	-2.432
72.242	3.551	72.156	-1.954
76.998	2.934	76.909	-1.471
81.701	2.297	81.616	-1.003
86.350	1.662	86.279	-.573
90.948	1.049	90.899	-.216
95.497	.484	95.473	.022
100.000	.048	100.000	.048



TABLE II

NACELLE DETAILS

Nacelle position	Inlet area (sq in.)	Exit area (sq in.)	Frontal area (sq in.)	Length (in.)	Maximum diameter (in.)	Model scale
Central inboard	8.12	9.08	40.715	36.00	7.20	1/6
Underslung inboard with normal inlet	8.12	9.08	40.715	36.00	7.20	1/6
Underslung inboard with swept inlet	8.12	9.08	40.715	36.00	7.20	1/6
Tip	5.81	6.70	29.913	30.85	6.17	1/7



TABLE III

SUMMARY OF FORCE AND RAM-RECOVERY CHARACTERISTICS

Model designation	$\frac{V_1}{V_0}$	$\frac{dC_L}{d\alpha}$	Approximate C_L for unstable break in C_M	$\alpha_{C_L=0}$ (deg)	$\frac{dC_M}{dC_L}$	C_L at $\alpha=20^\circ$	C_{DF}		Ram-recovery ratio	
							$C_L=0$	$C_L=0.5$	$\alpha=0^\circ$	$\alpha=6^\circ$
Plain wing	--	0.067	0.78	-1.2	-0.020	1.01	----	----	--	--
Wing with nacelle in central inboard position	0	.069	.85	-.9	-.022	--	0.075	0.071	0.80	0.71
	.3	.069	--	-1.0	----	1.11	----	----	.99	.96
	.6	----	--	--	----	--	.046	.049	.99	.98
	.64	.069	.90	-1.1	-.022	1.11	----	----	--	--
	.9	----	--	--	----	--	----	----	.95	.94
	1.2	----	--	--	----	--	----	----	.85	.85
Wing with nacelle in underslung inboard position with normal inlet	0	.067	.70	-1.1	-.021	1.03	.071	.069	.91	.97
	.3	.066	--	-1.0	----	1.02	----	----	.99	.99
	.6	----	--	--	----	--	.032	.031	.99	.99
	.73	.067	.91	-1.1	-.021	1.04	----	----	--	--
	.9	----	--	--	----	--	----	----	.99	.99
	1.2	----	--	--	----	--	----	----	.99	.99
Wing with nacelle in underslung inboard position with swept inlet	0	.067	.90	-1.0	-.032	1.01	.100	.105	.92	.88
	.3	.067	--	-.9	----	1.03	----	----	.98	.98
	.6	----	--	--	----	--	.036	.036	.98	.98
	.73	.067	.90	-.9	-.032	1.02	----	----	--	--
	.9	----	--	--	----	--	----	----	.96	.96
	1.2	----	--	--	----	--	----	----	.93	.92
Wing with nacelle in tip position	0	.071	.80	-1.1	-.068	1.03	.047	.047	.99	.99
	.3	.071	--	-1.1	----	1.06	----	----	.99	.99
	.6	----	--	--	----	--	.031	.028	.98	.98
	.83	.072	.82	-1.0	-.068	1.05	----	----	--	--
	.9	----	--	--	----	--	----	----	.96	.96
	1.2	----	--	--	----	--	----	----	.95	.95



TABLE IV

VALUES OF CRITICAL MACH NUMBER AS DETERMINED
BY THE KARMAN-TSIEN HODOGRAPH METHOD
OF REFERENCE 6

Critical Mach number	Pressure coef- ficient for Mach number approaching zero
1.000	0
.932	-.05
.884	-.1
.845	-.15
.816	-.2
.769	-.3
.730	-.4
.698	-.5
.670	-.6
.622	-.8
.583	-1.0
.511	-1.5
.461	-2.0
.394	-3.0
.349	-4.0



Wing area = 8.283 square feet (semispan)
 Aspect ratio = 6.04 (based on full span)
 $\bar{c} = 20.736$ inches (parallel to root chord)
 Taper ratio = 0.5

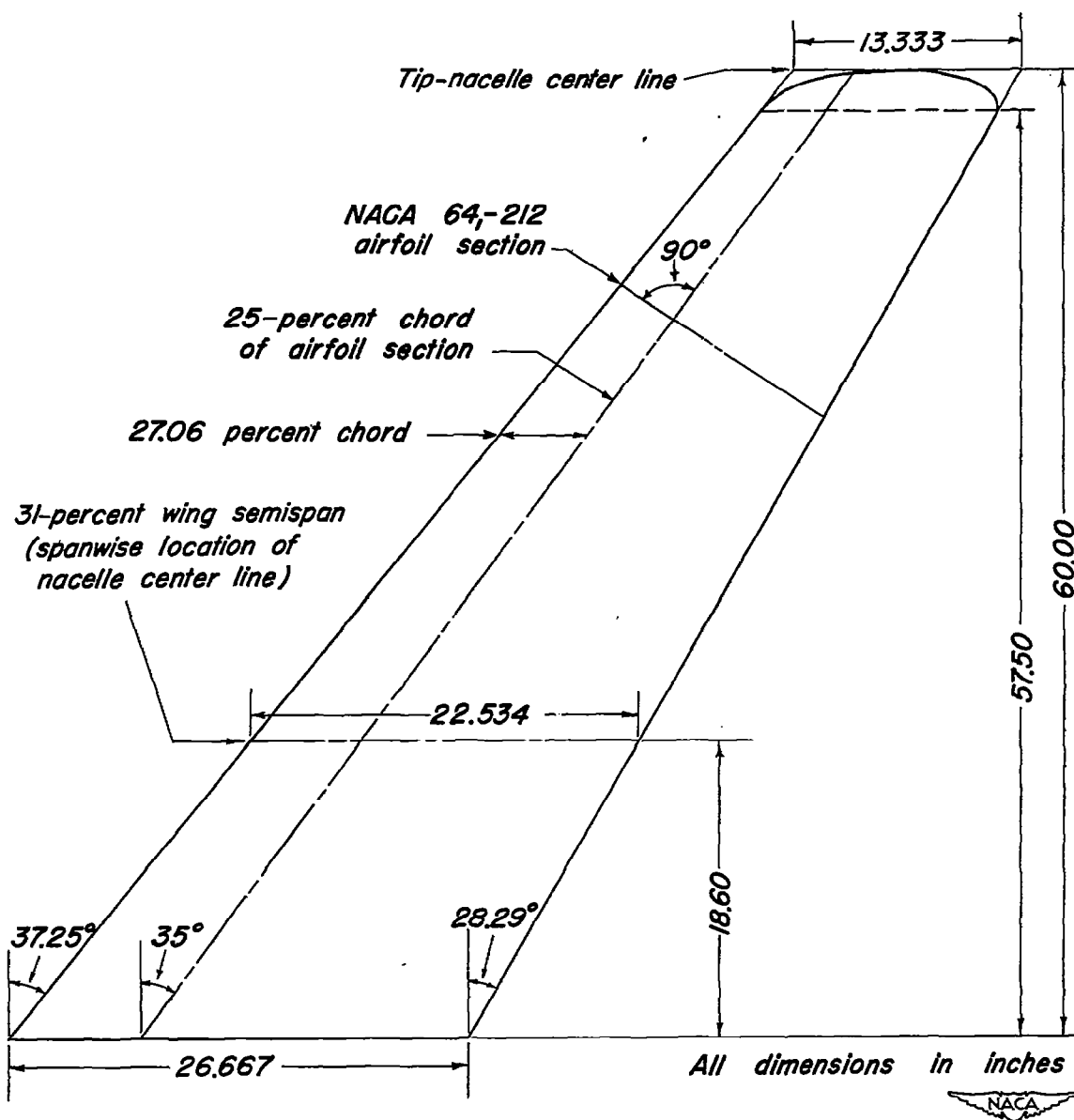
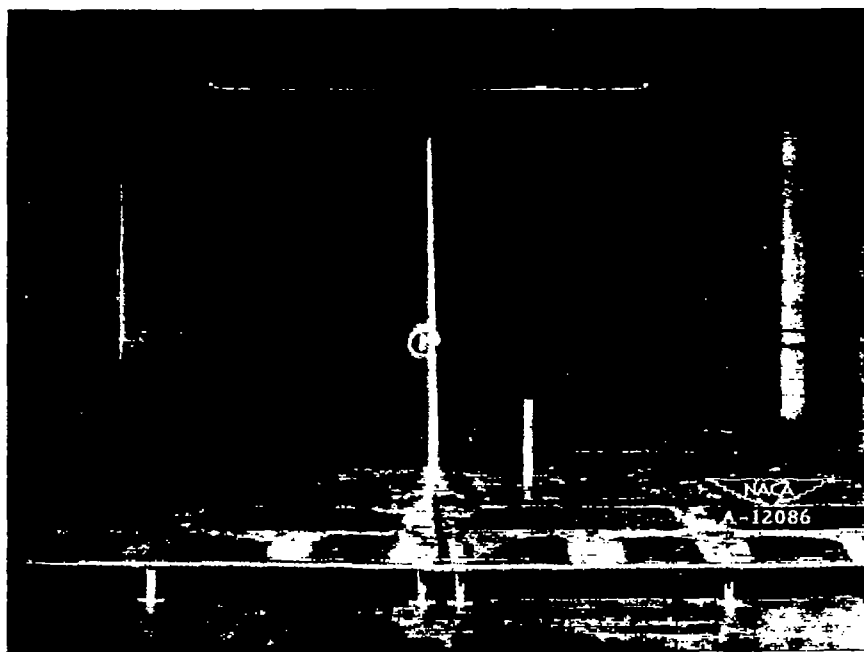


Figure 1.- Plan form of model wing.



(a) Front view of wing with nacelle in underslung inboard position.



(b) Upper surface of wing with nacelle in underslung inboard position.

Figure 2.- Installation of wing with nacelle in inboard position in one of the Ames 7- by 10-foot wind tunnels.



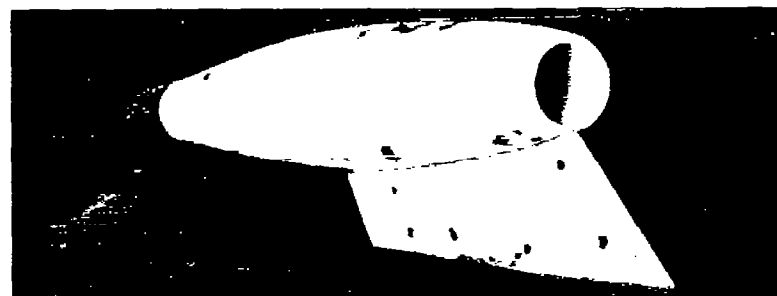
(a) Central inboard position.



(b) Underslung inboard position with normal inlet.



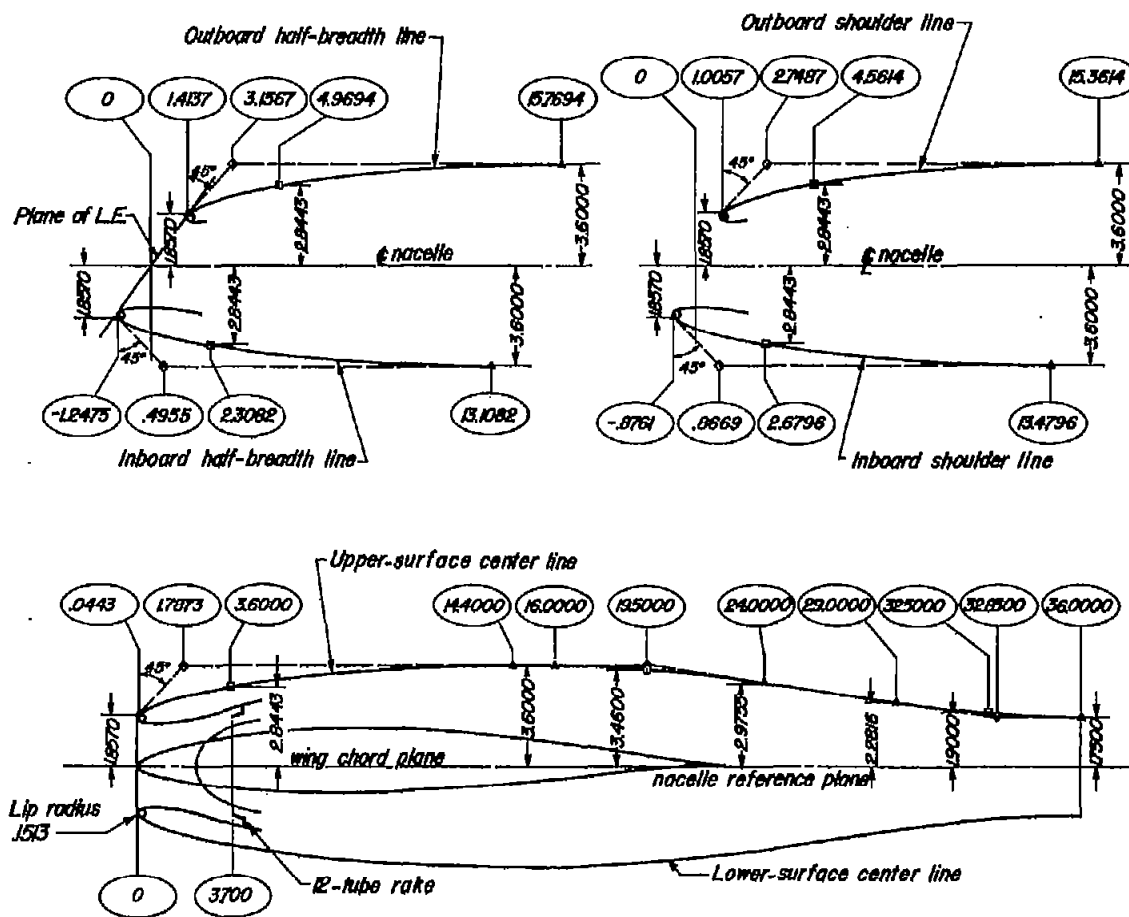
(c) Underslung inboard position with swept inlet.



(d) Tip position.

NACA
A-13440

Figure 3.- Nacelle in various positions on the wing.



Note:

1. Forebody identical upper and lower
2. Afterbody (station 16 to 36, is circular
3. Control lines straight between tangent points
4. All dimensions given in inch model scale
5. Jet-unit entry, approximate station 7.5
6. Nacelle frontal area, 40.7 square inches

Legend:

- ▲ Tangent point
- ◆ Intersection of tangent lines
- Shoulder point

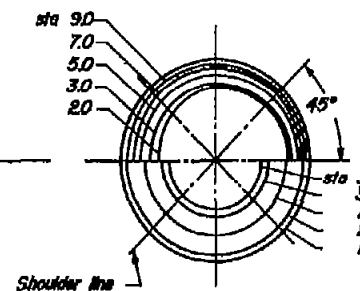
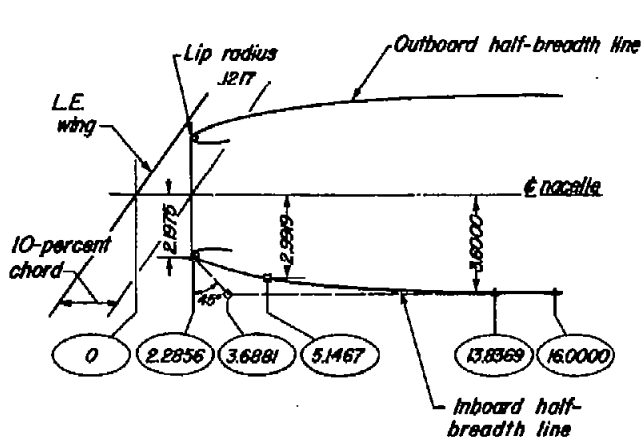


Figure 4.- Control line drawing for nacelle tested in central inboard position.



Note:

1. Upper forward body above wing is formed by radii with centers at nacelle center line on nacelle reference plane
2. Inboard external lines forward of station 6.5 which lie between nacelle reference plane and wing lower surface are formed of lines normal to nacelle reference plane and tangent to the half-breadth
3. Outboard external lines forward of station 10.5 which lie between nacelle reference plane and wing lower surface are formed of lines normal to nacelle reference plane and tangent to the half-breadth
4. Afterbody (station 16 to 36) is circular

5. Lower forebody (station 2.25 to 16) is symmetrical about vertical center plane
6. Jet-unit entry approximately station 7.5
7. Control lines straight between tangent points
8. All dimensions given in inches model scale
9. Nacelle frontal area, 40.715 square inches

Legend:

- ▲ Tangent point
- ◆ Intersection of tangent lines
- Shoulder point

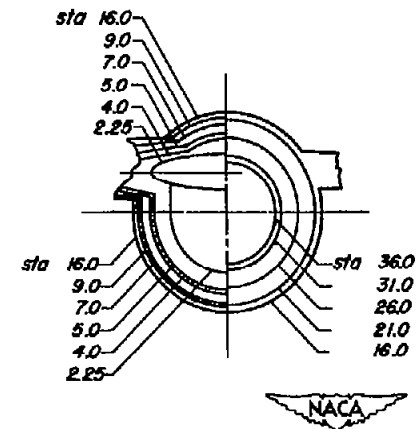
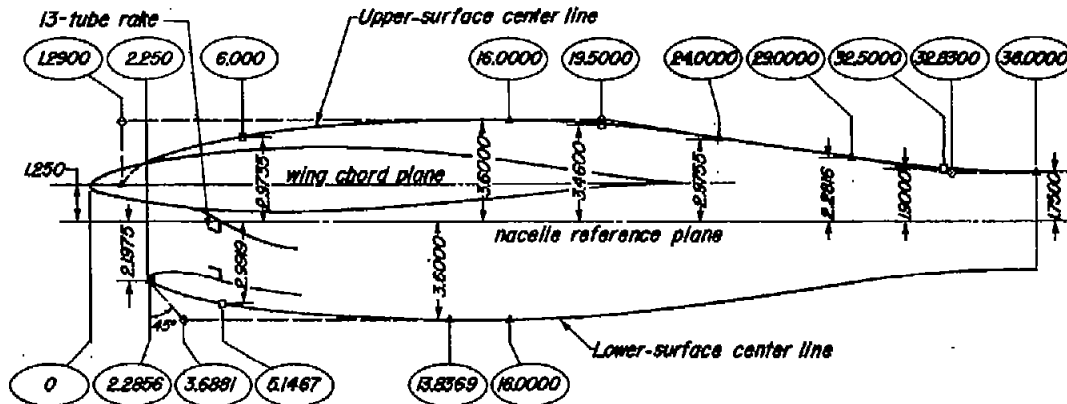
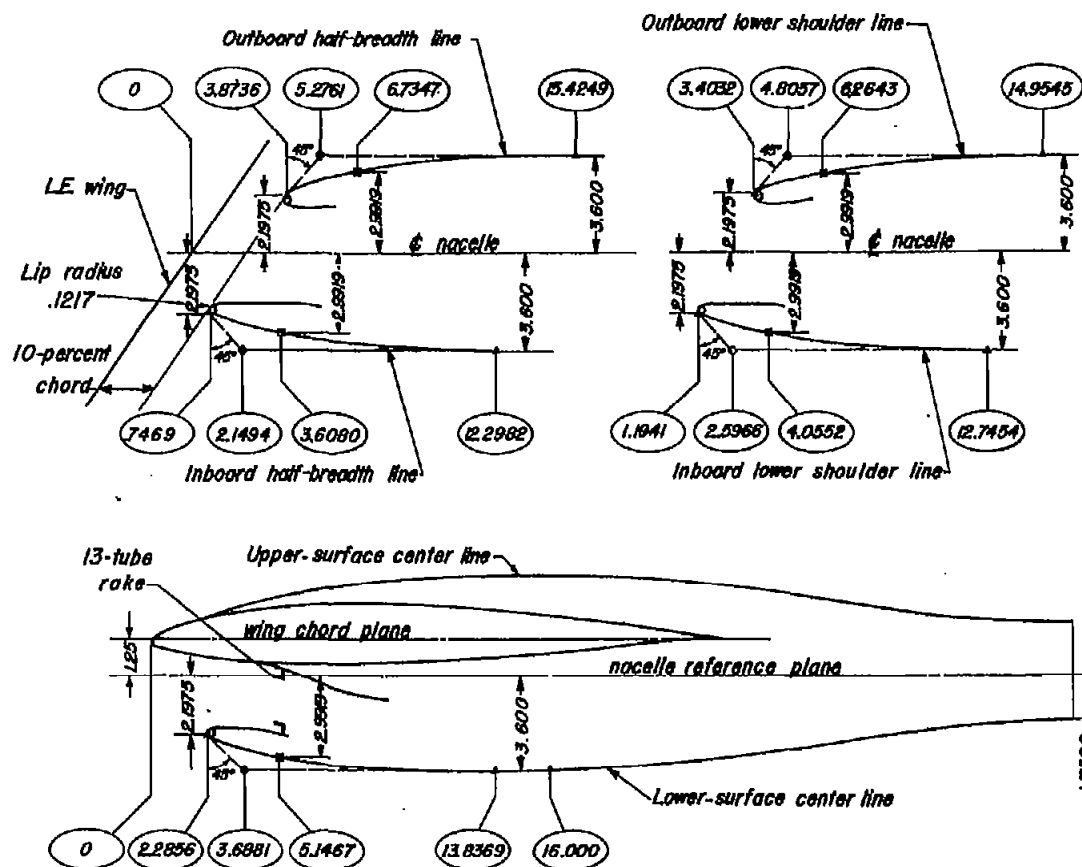


Figure 5.- Control line drawing for nacelle tested in underslung inboard position with normal inlet.

**Note:**

1. Inboard external lines forward of station 6.5 which lie between nacelle reference plane and wing lower surface are formed of lines normal to nacelle reference plane and tangent to the halfbreadth
2. Outboard external lines forward of station 10.5 which lie between nacelle reference plane and wing lower surface are formed of lines normal to nacelle reference plane and tangent to the half breadth
3. Control lines straight between tangent points
4. All dimensions given in inches model scale
5. Nacelle frontal area, 40.715 square inches
6. Jet-unit entry approximately station 7.5

Legend:

- ▲ Tangent point
- ◆ Intersection of tangent lines
- Shoulder point

Figure 6.-Control line drawing for nacelle tested in underslung inboard position with swept inlet.

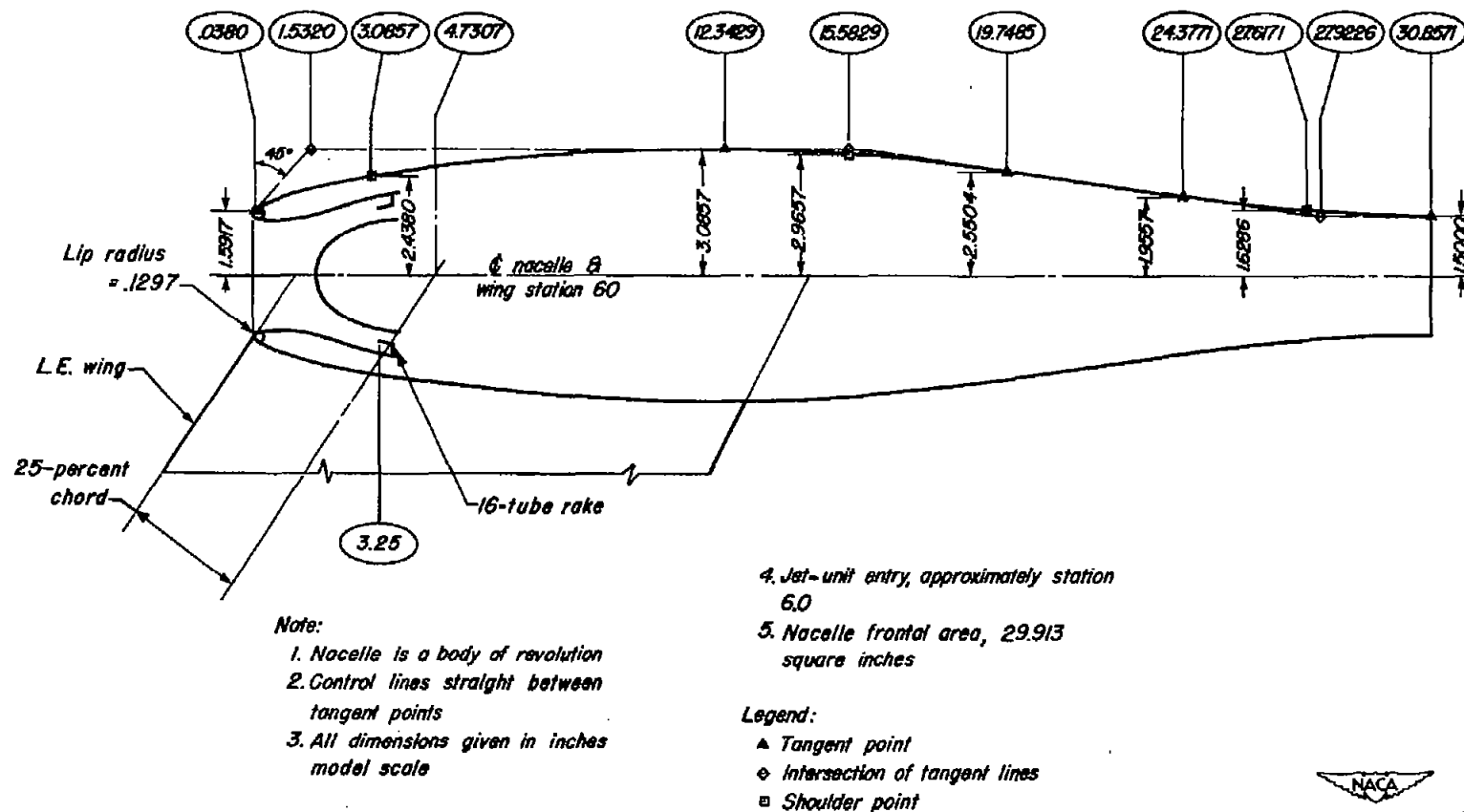


Figure 7.- Control line drawing for nacelle tested at wing tip.

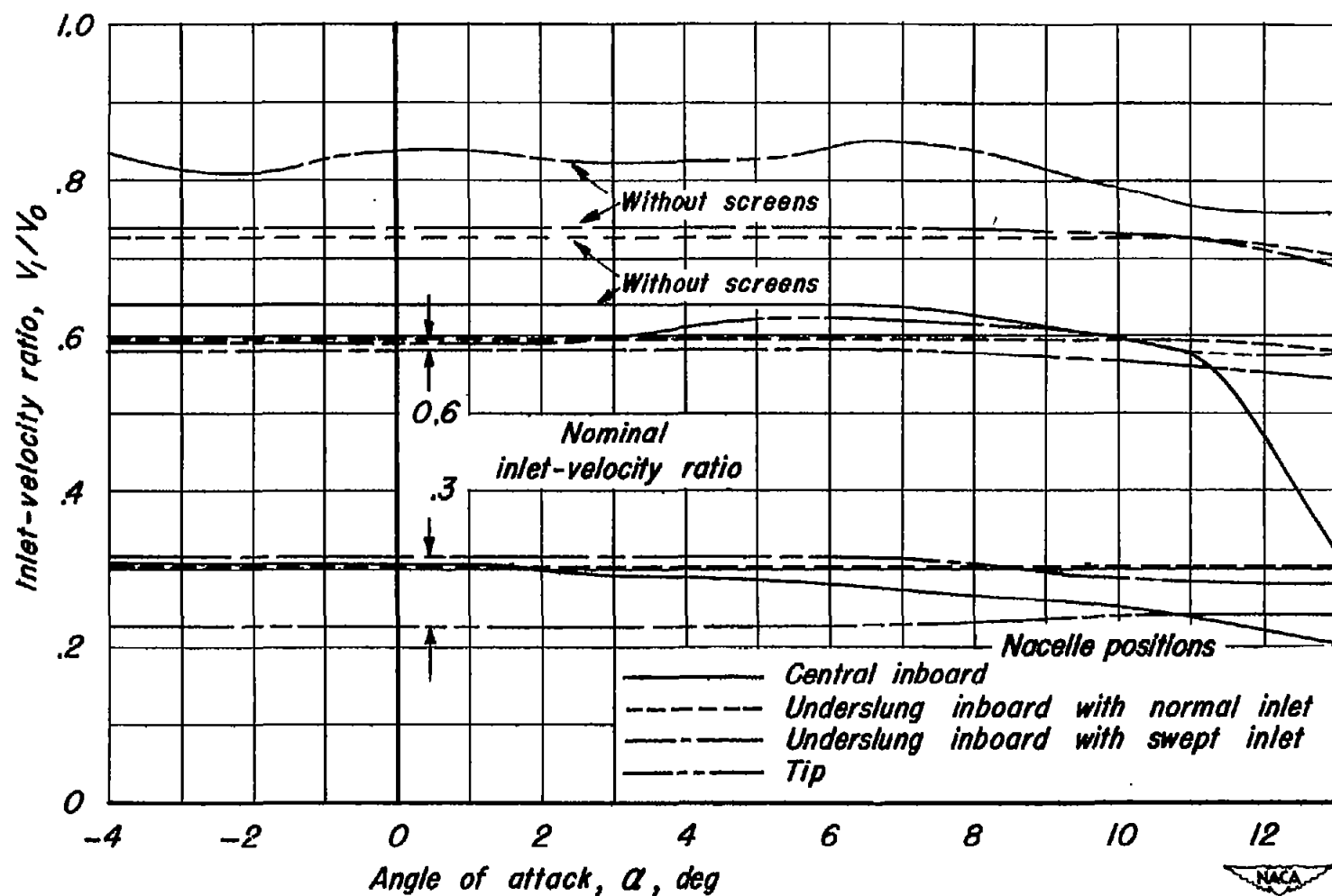


Figure 8.—Variation of inlet-velocity ratio with angle of attack during force tests for the nacelle in the various positions on the wing.

•

•

•

•

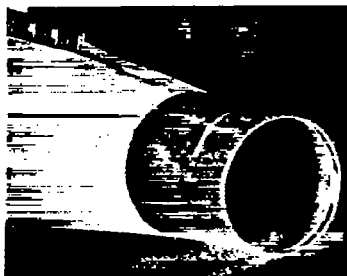
•

•

•

•

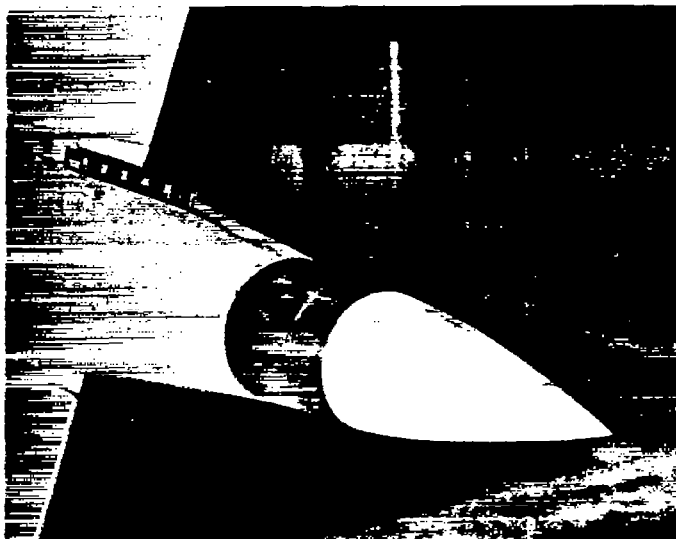
•



(a) Open.



(b) Flush plug.



(c) Fairing plug.

NACA
A-12041

Figure 9.— Detail of tail-pipe outlet.

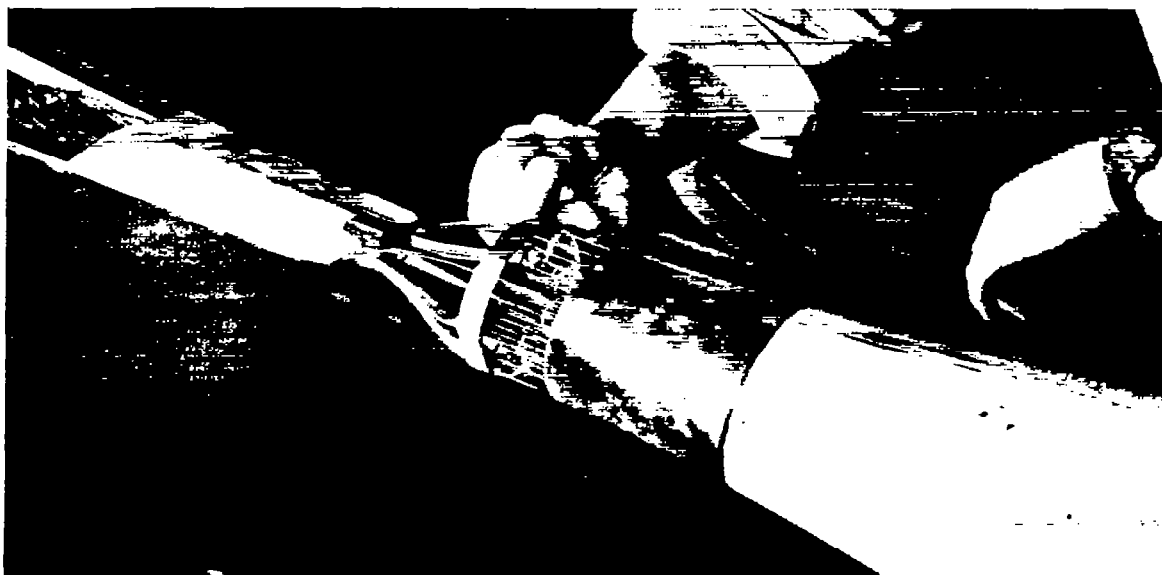


Figure 10.— Detail of tail-pipe pressure rake.

NACA
A-12081

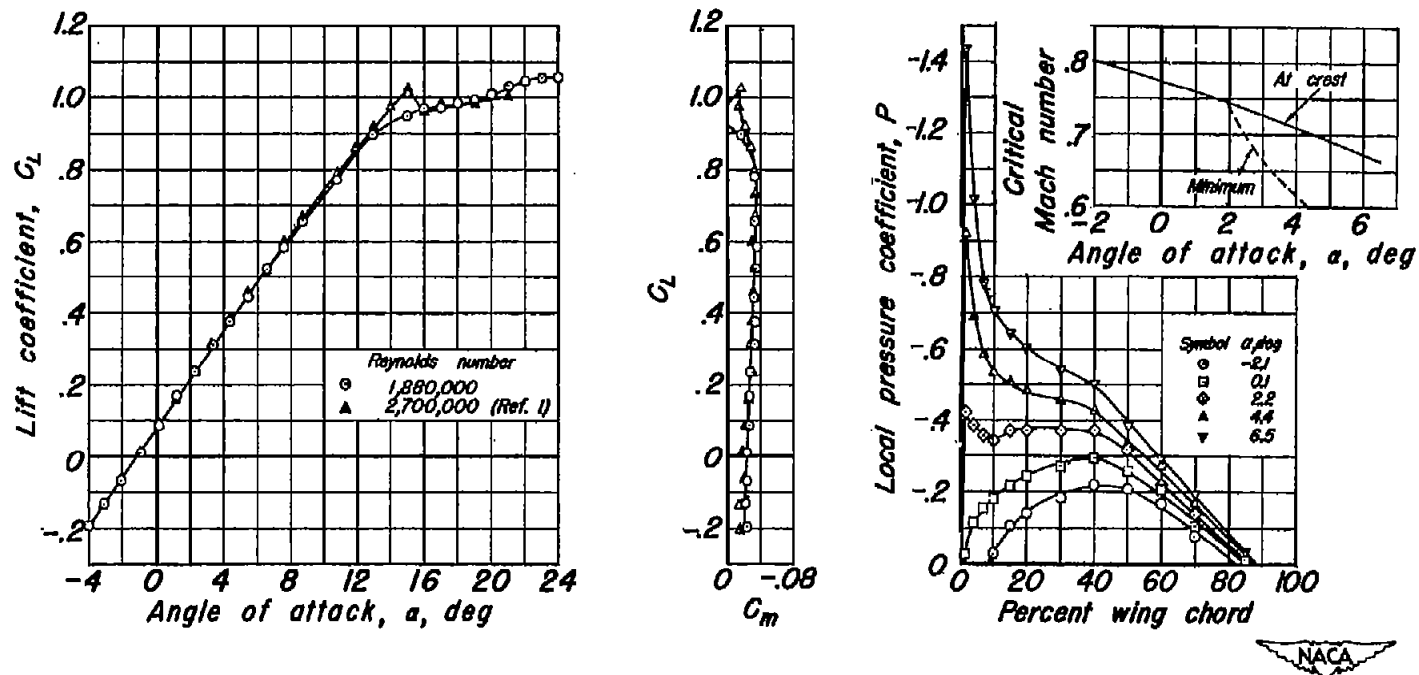
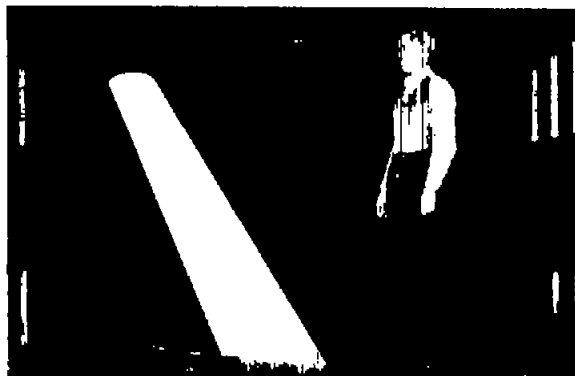


Figure 11.—Lift and pitching-moment characteristics of the plain wing and the upper-surface pressure distribution and critical Mach number at the 0.31-percent semispan station.

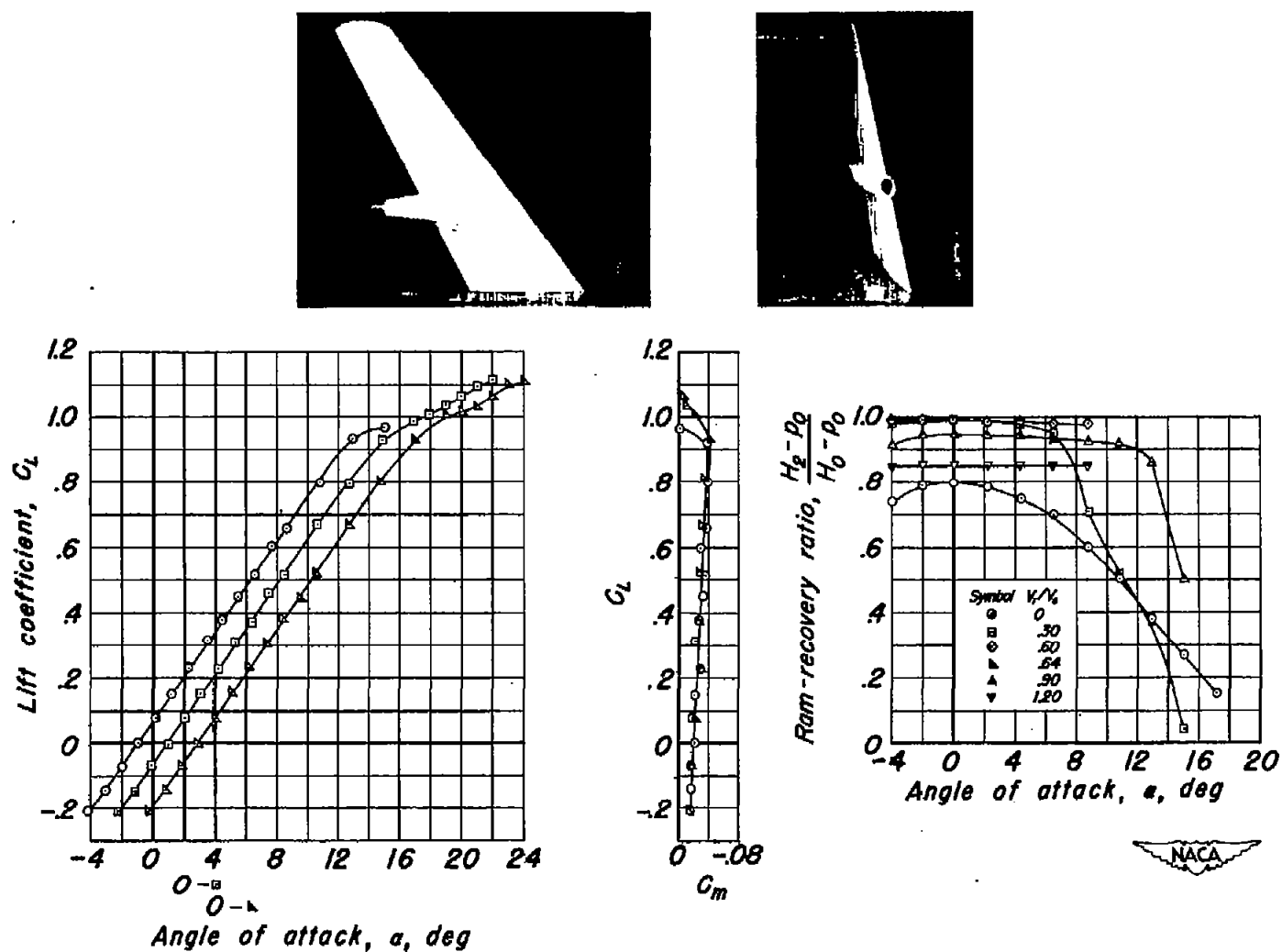


Figure 12.—Lift, pitching-moment, and ram-recovery characteristics of the wing and nacelle with the nacelle in the central inboard position.

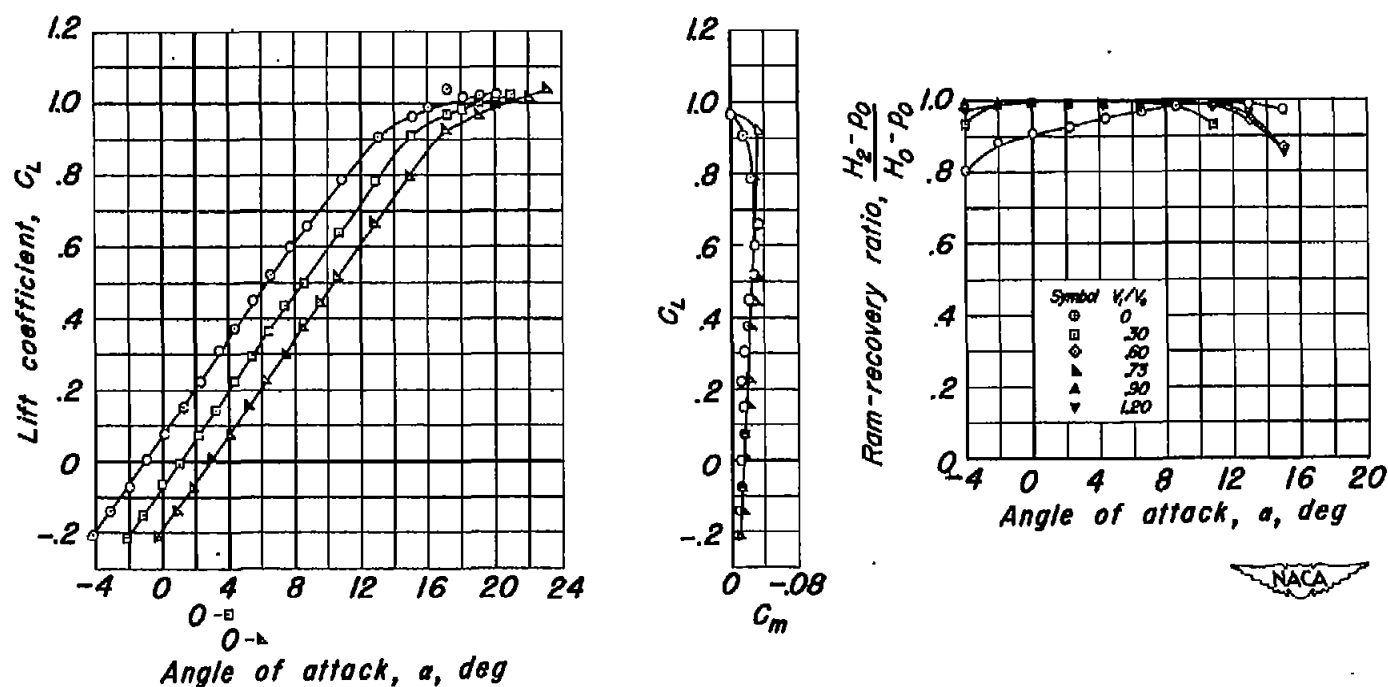


Figure 13.—Lift, pitching-moment, and ram-recovery characteristics of the wing and nacelle with the nacelle in the underslung inboard position with normal inlet.

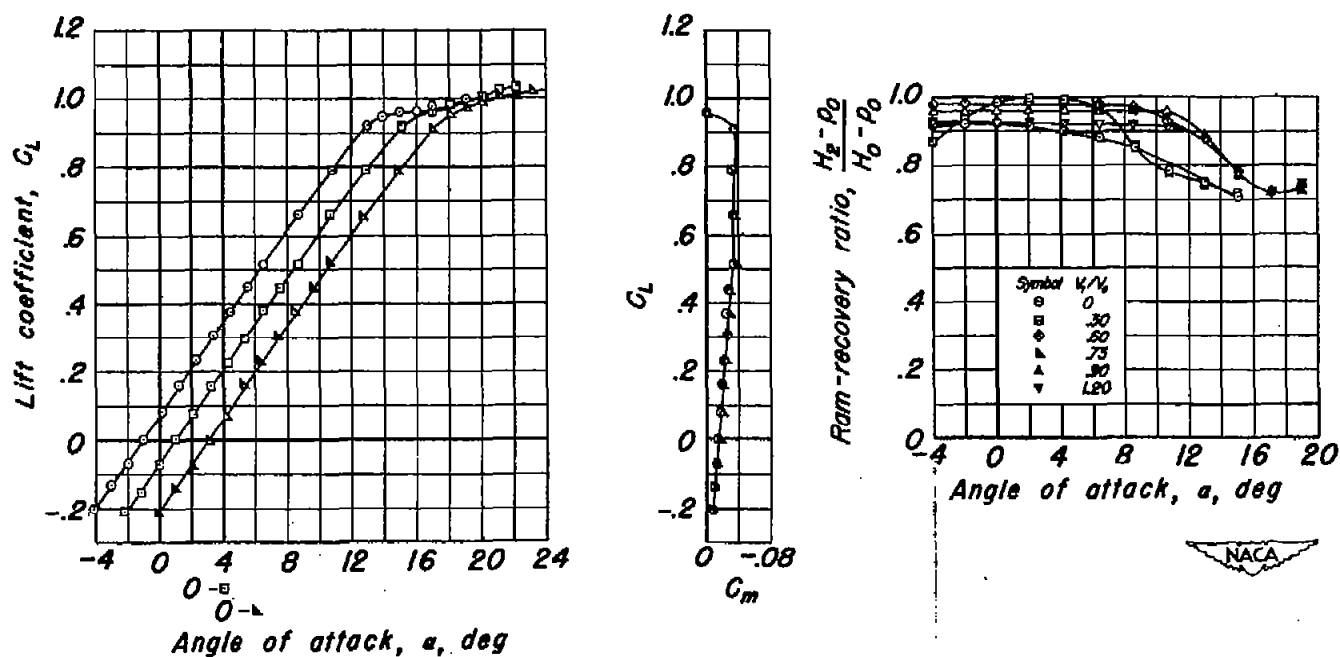


Figure 14.—Lift, pitching-moment, and ram-recovery characteristics of the wing and nacelle with the nacelle in the underslung position with swept inlet.

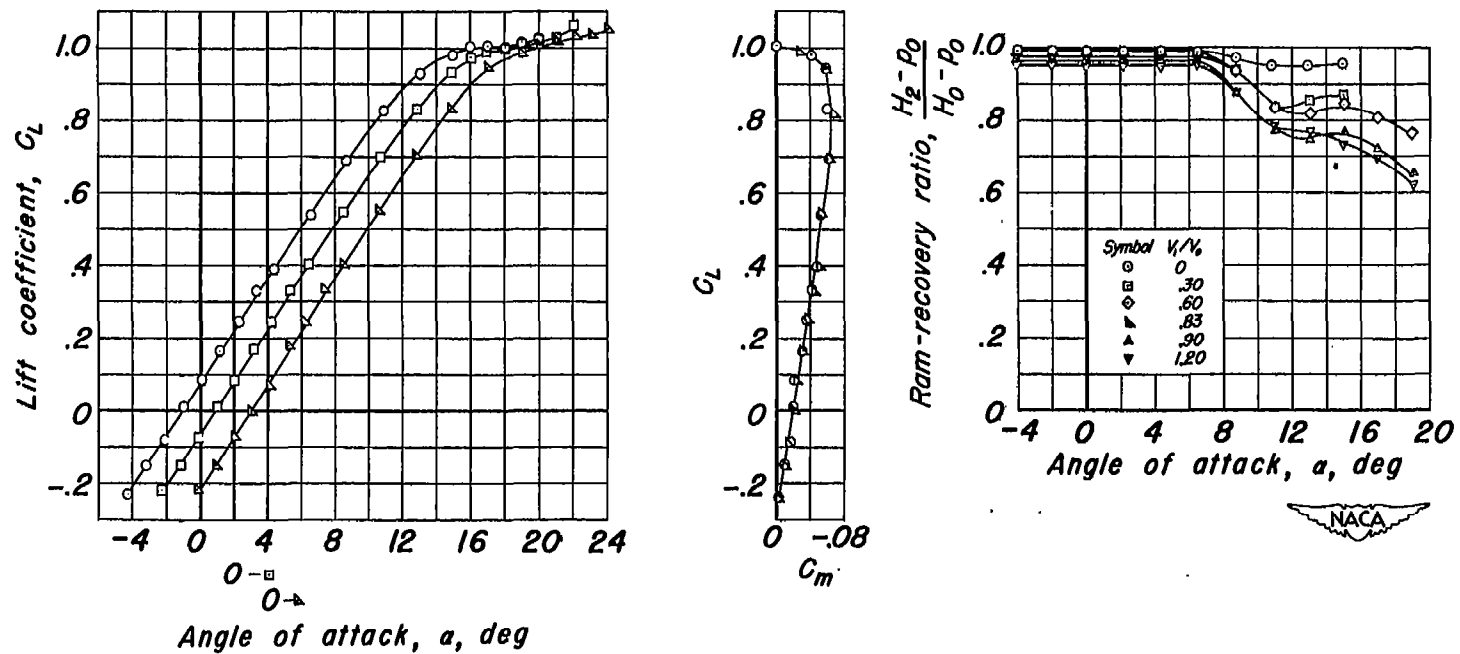
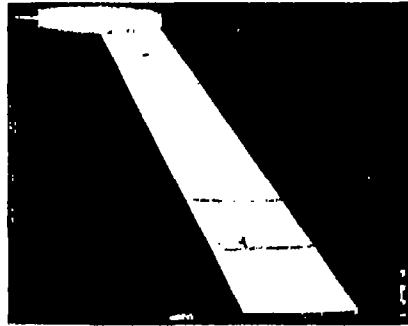


Figure 15.—Lift, pitching-moment, and ram-recovery characteristics of the wing and nacelle with the nacelle in the tip position.

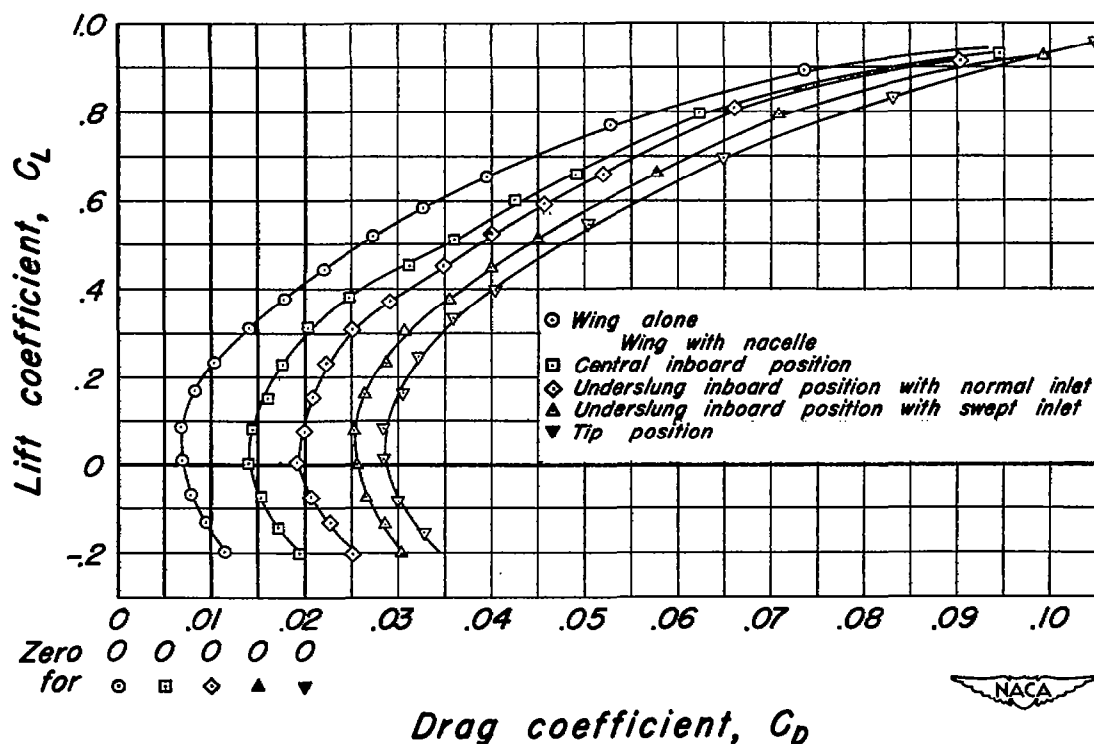


Figure 16.—Total drag characteristics of the wing and wing-nacelle combinations. V_1/V_0 , 0.

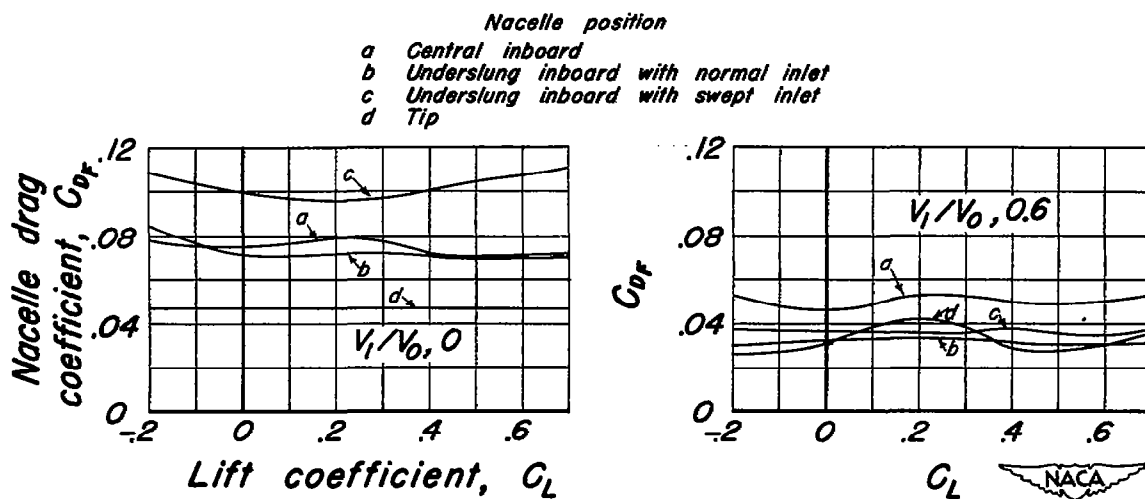


Figure 17.—Drag characteristics of the nacelle.

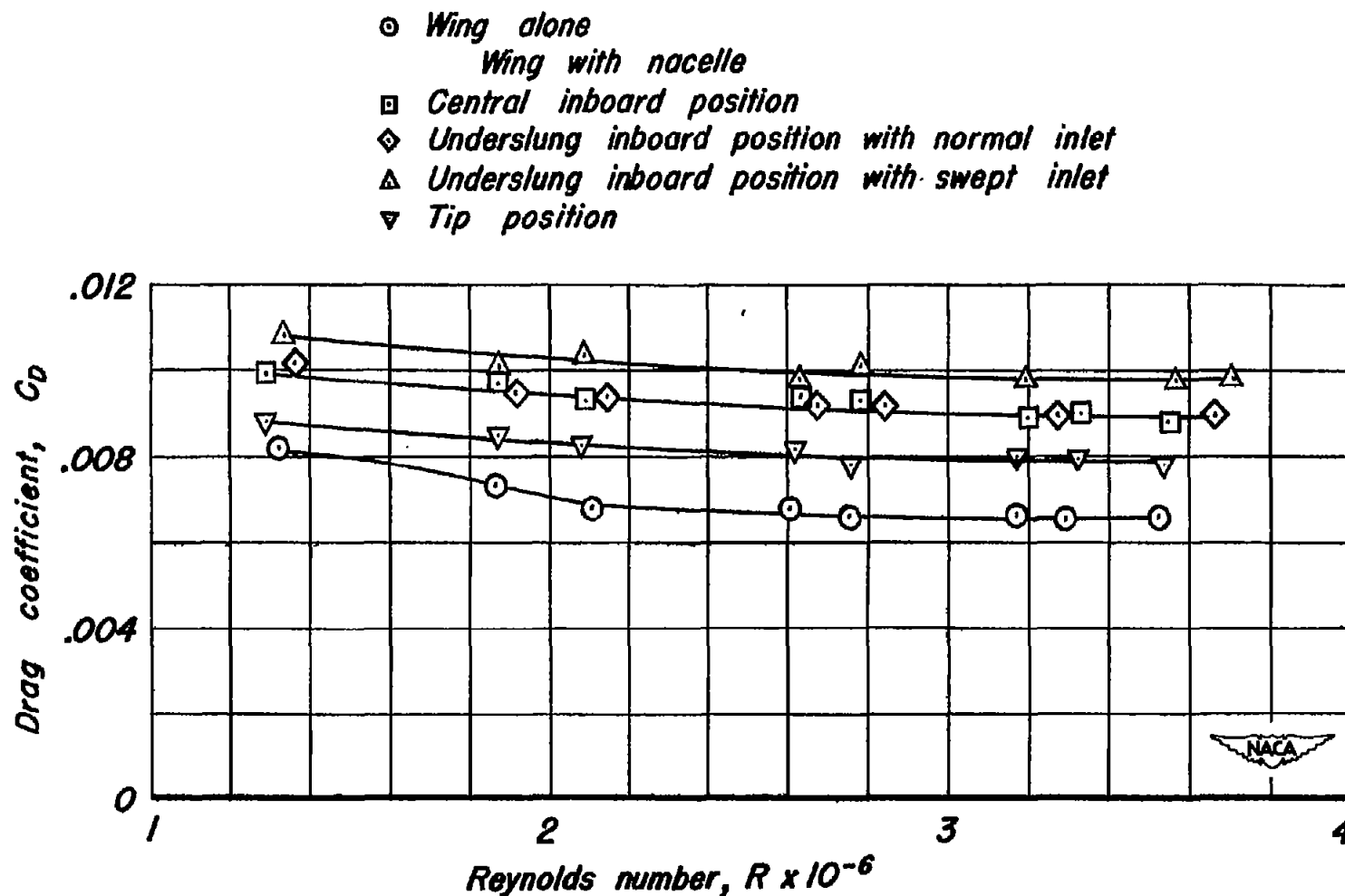
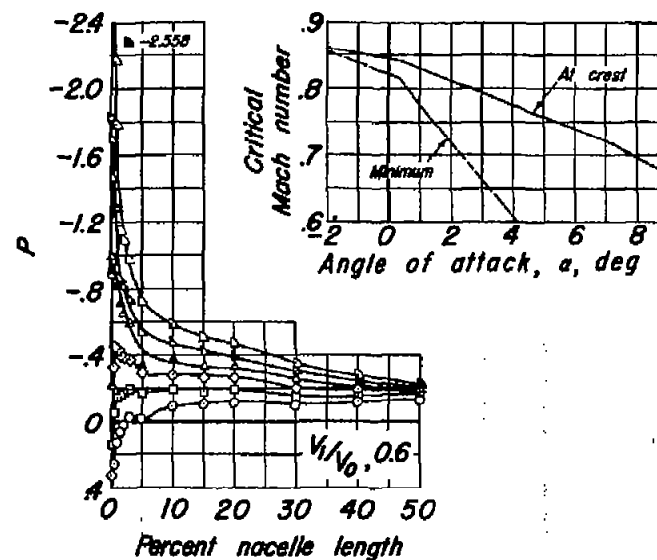
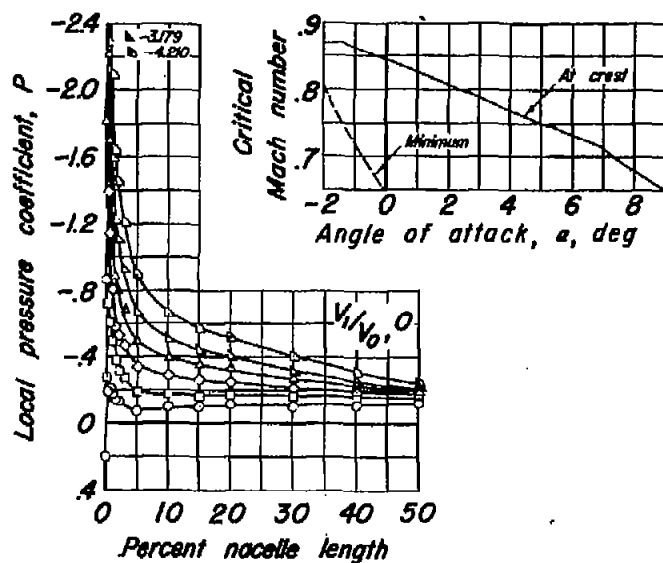
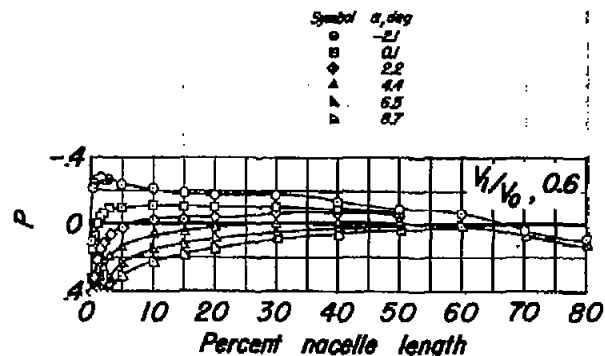
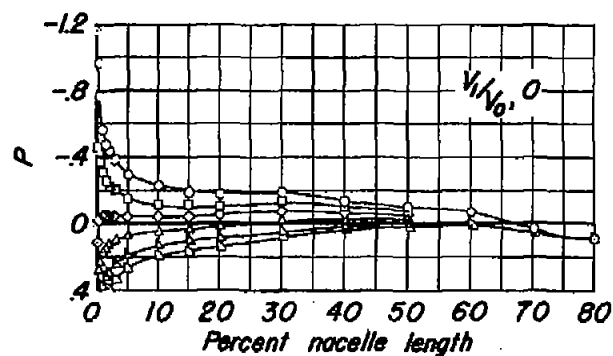


Figure 18.— Variation of drag coefficient with Reynolds number for the wing and wing-nacelle combinations. V_i/V_0 , 0 and α , 0° .

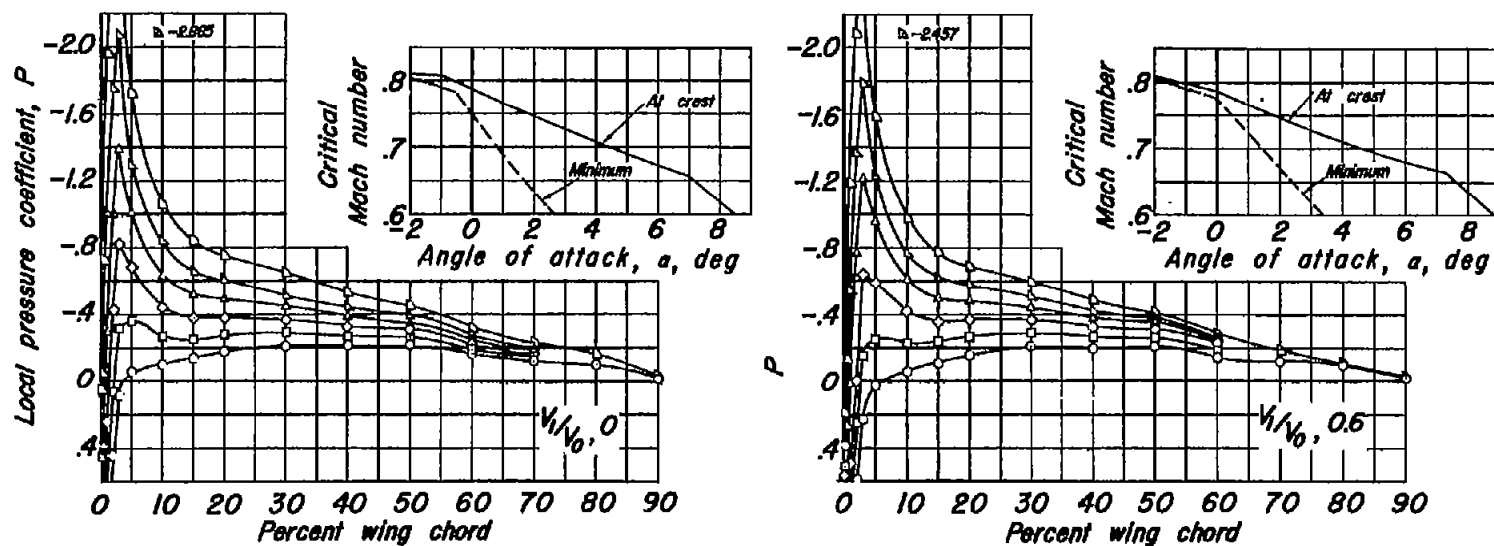


(a) Upper-surface center line.

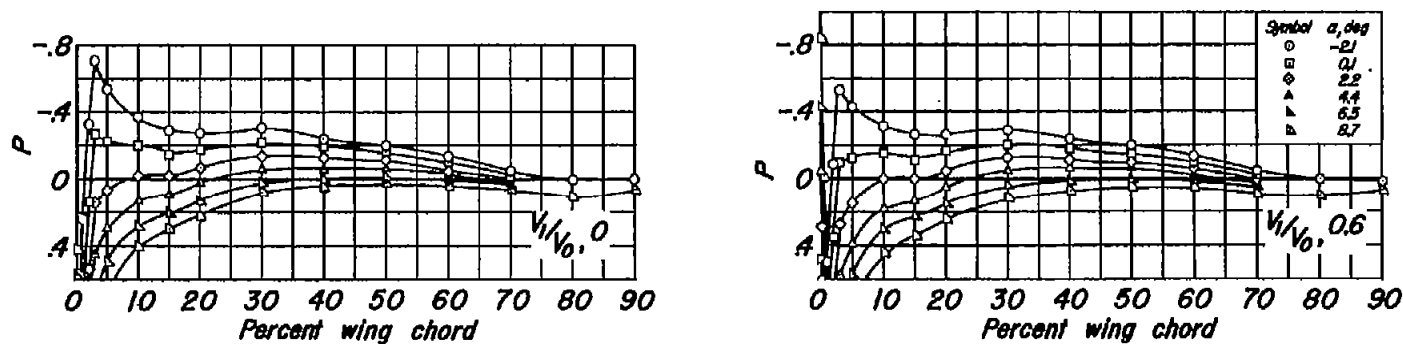


(b) Lower-surface center line.

Figure 19.—Pressure distribution and critical Mach number for the nacelle in the central inboard position.

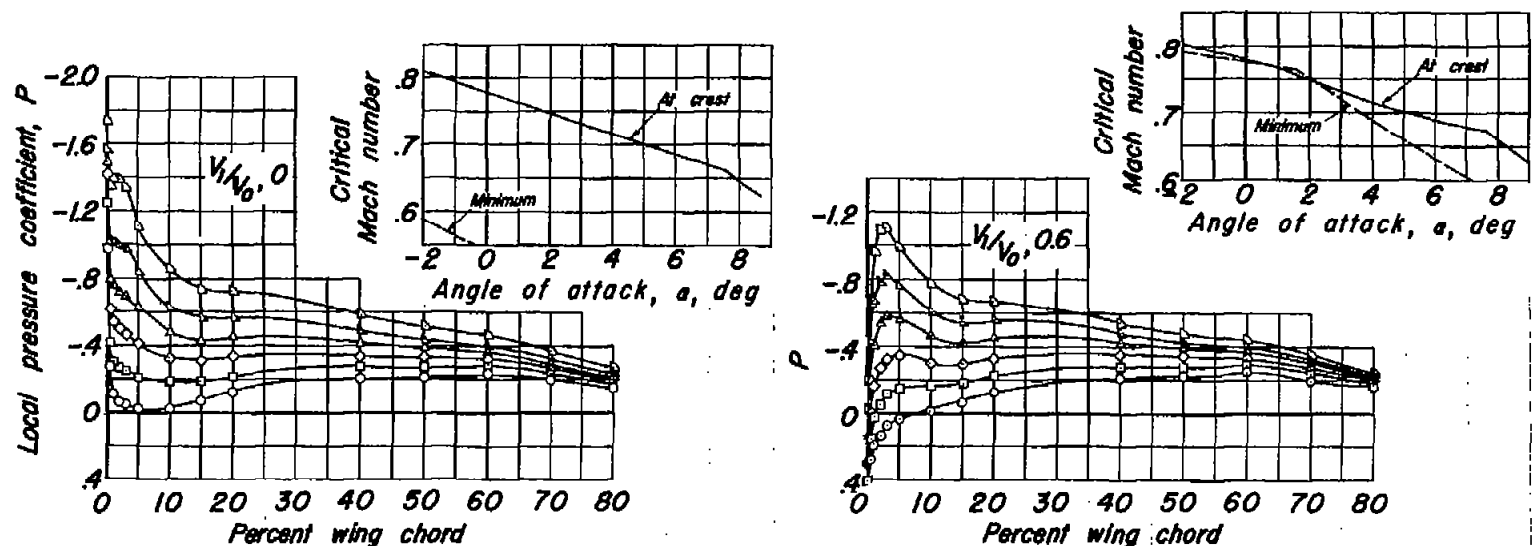


(c) Inboard upper wing-nacelle juncture.

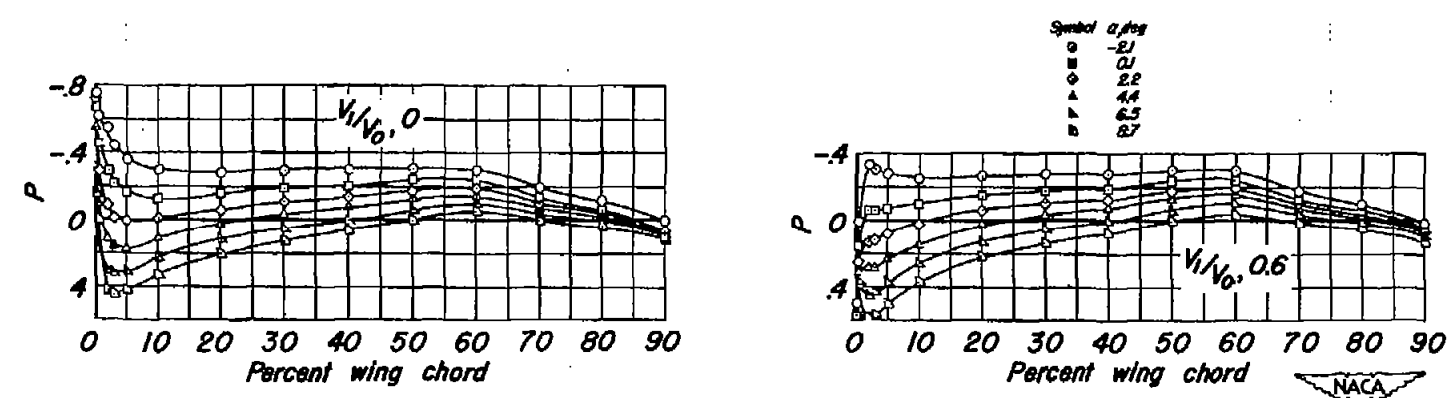


(d) Inboard lower wing-nacelle juncture.

Figure 19.- Continued.

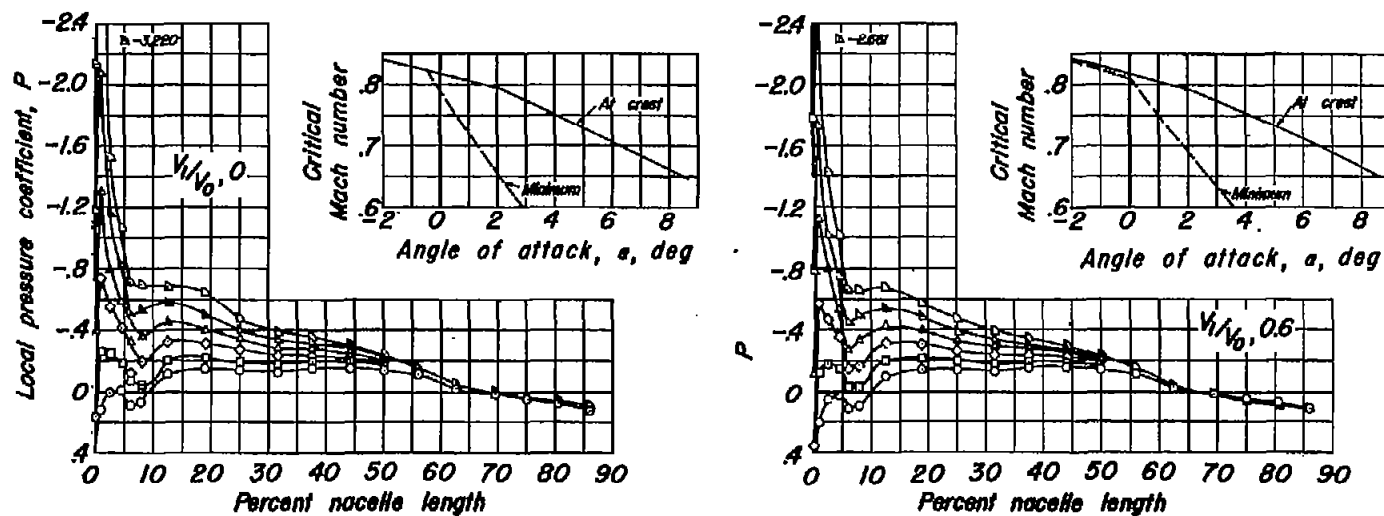


(e) Outboard upper wing-nacelle juncture.

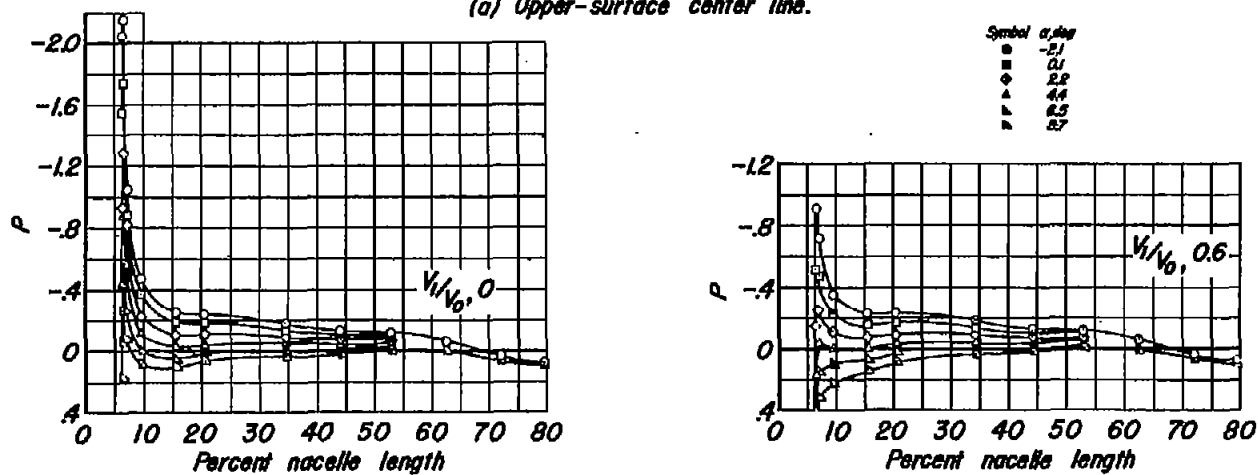


(f) Outboard lower wing-nacelle juncture.

Figure 19.—Concluded.

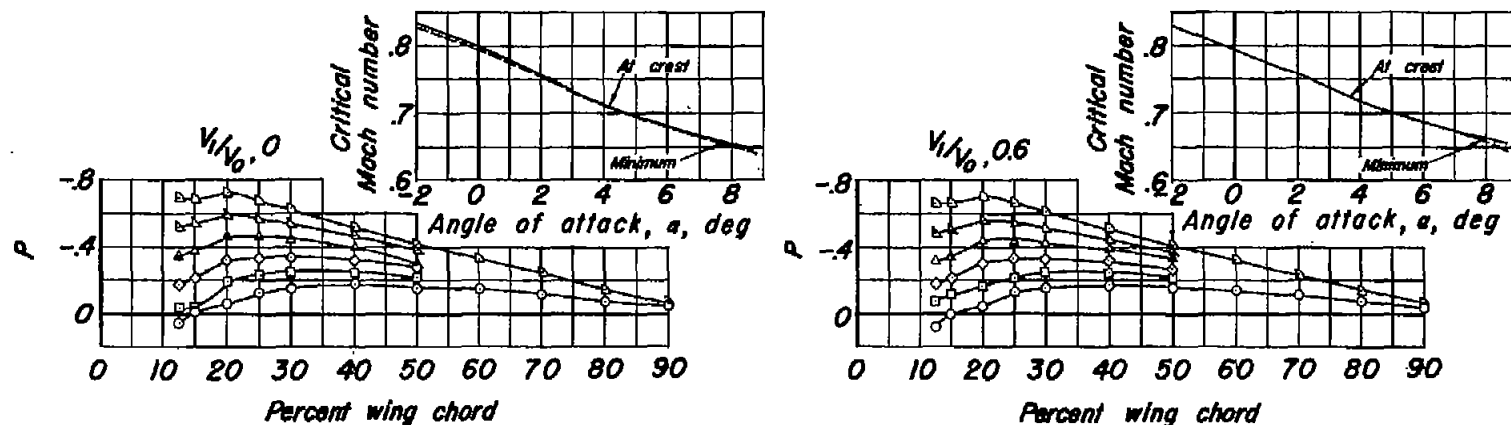


(a) Upper-surface center line.

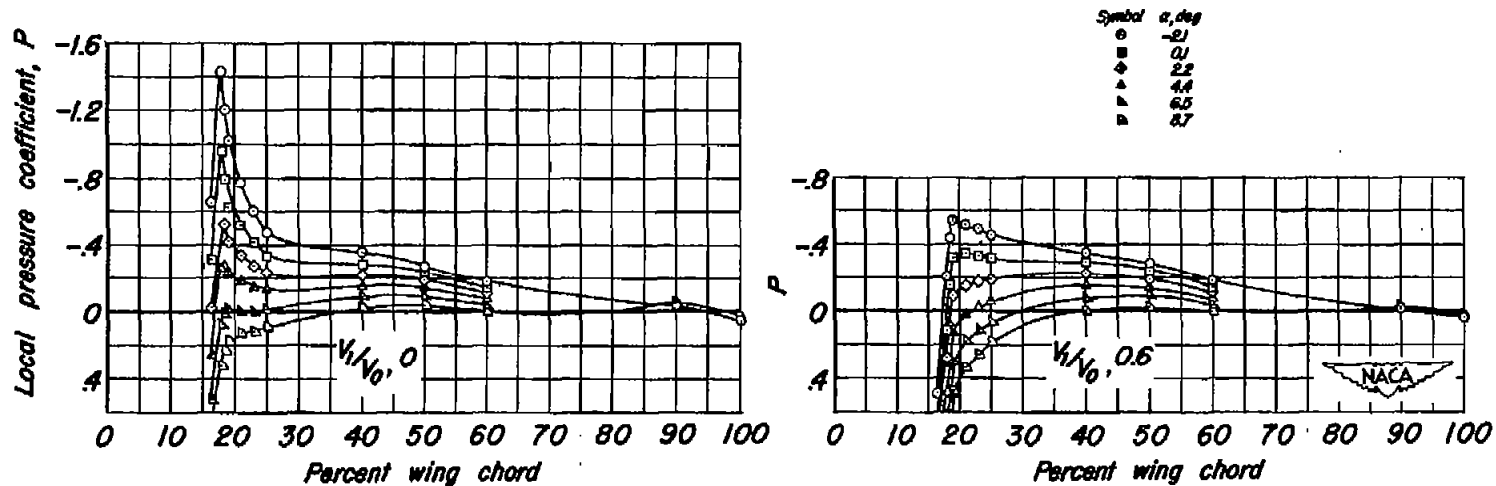


(b) Lower-surface center line.

Figure 20.—Pressure distribution and critical Mach number for the nacelle in the underslung inboard position with normal inlet.

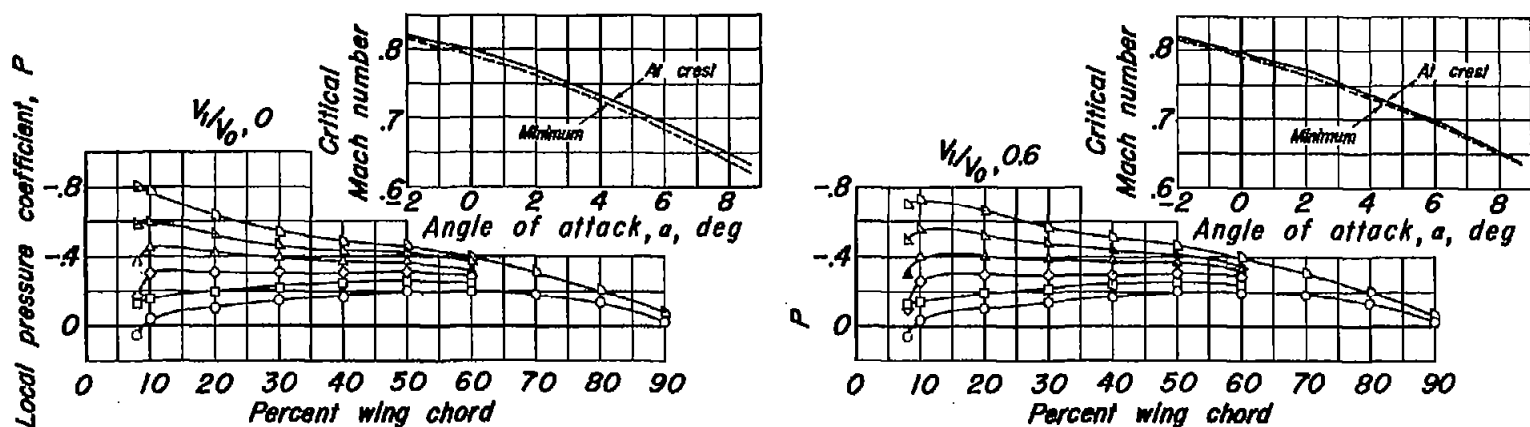


(c) Inboard upper wing-nacelle juncture.



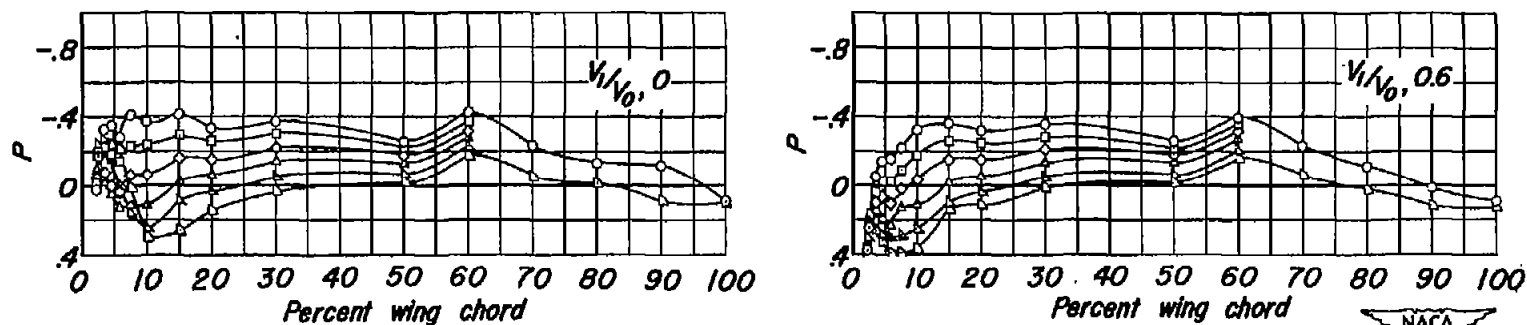
(d) Inboard lower wing-nacelle juncture.

Figure 20.- Continued.



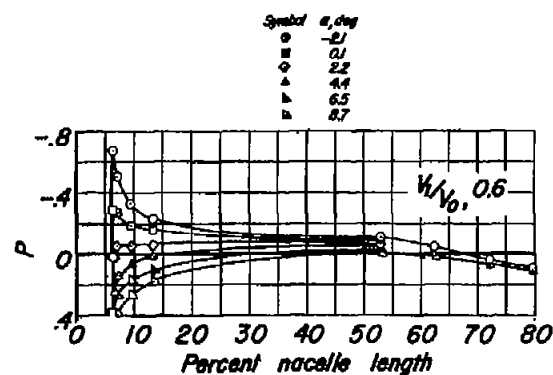
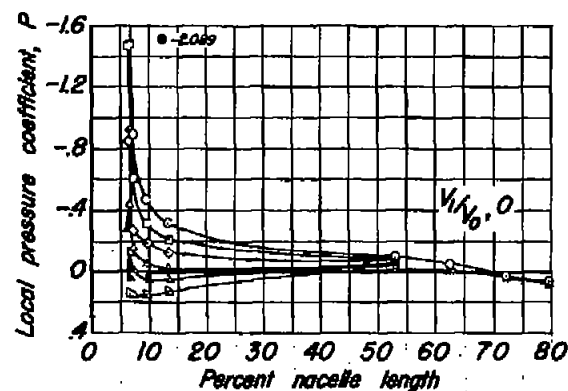
(e) Outboard upper wing-nacelle juncture.

Symbol	α , deg
○	-2.1
□	0.0
◇	2.2
△	4.4
▽	6.5
●	8.7

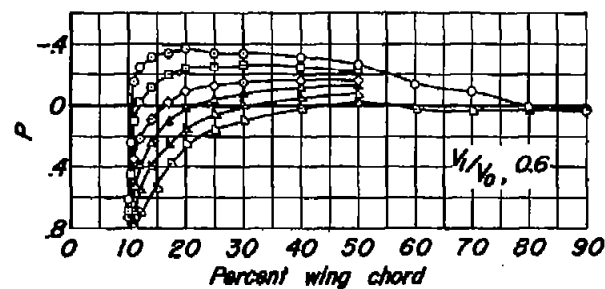
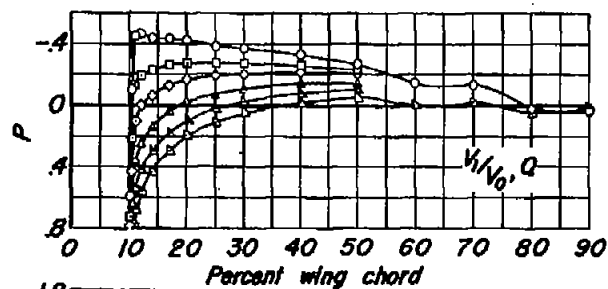


(f) Outboard lower wing-nacelle juncture.

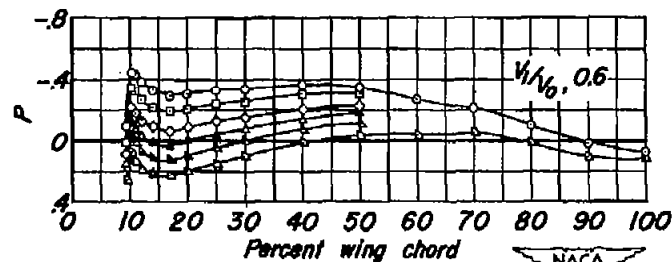
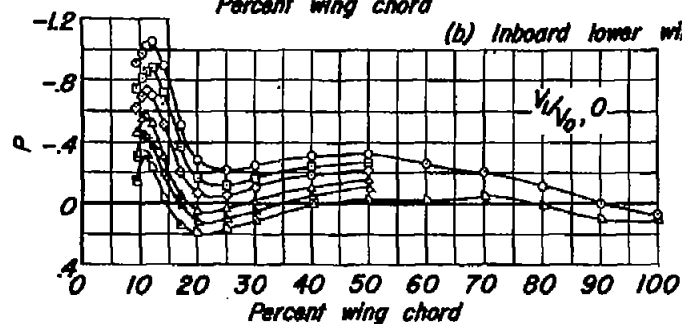
Figure 20.—Concluded.



(a) Lower-surface center line.

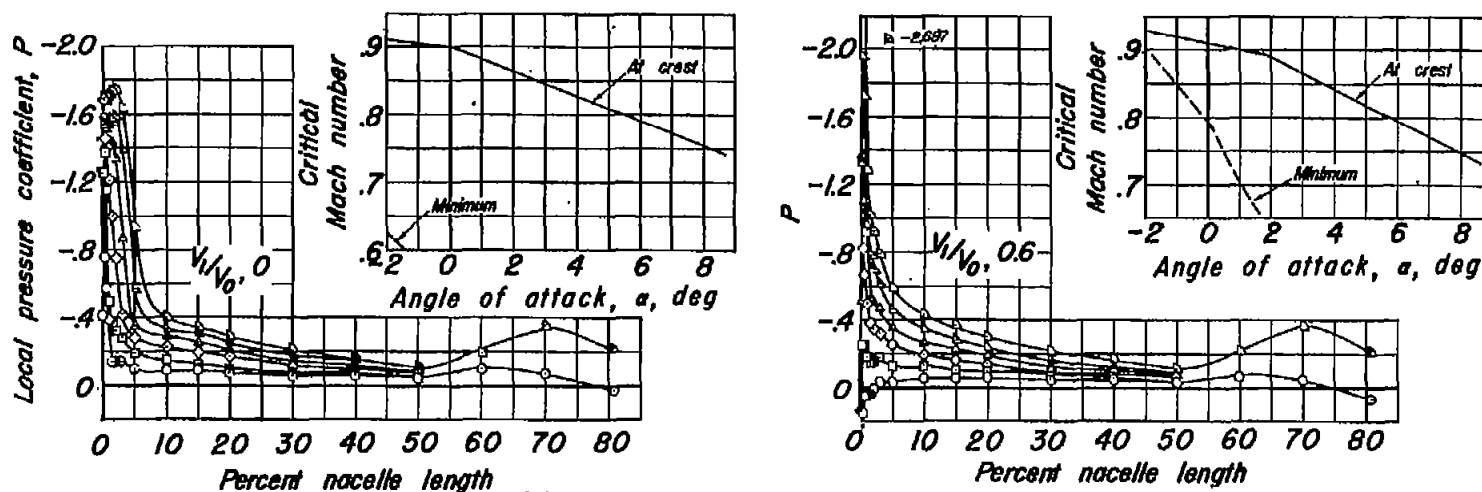


(b) Inboard lower wing-nacelle juncture.

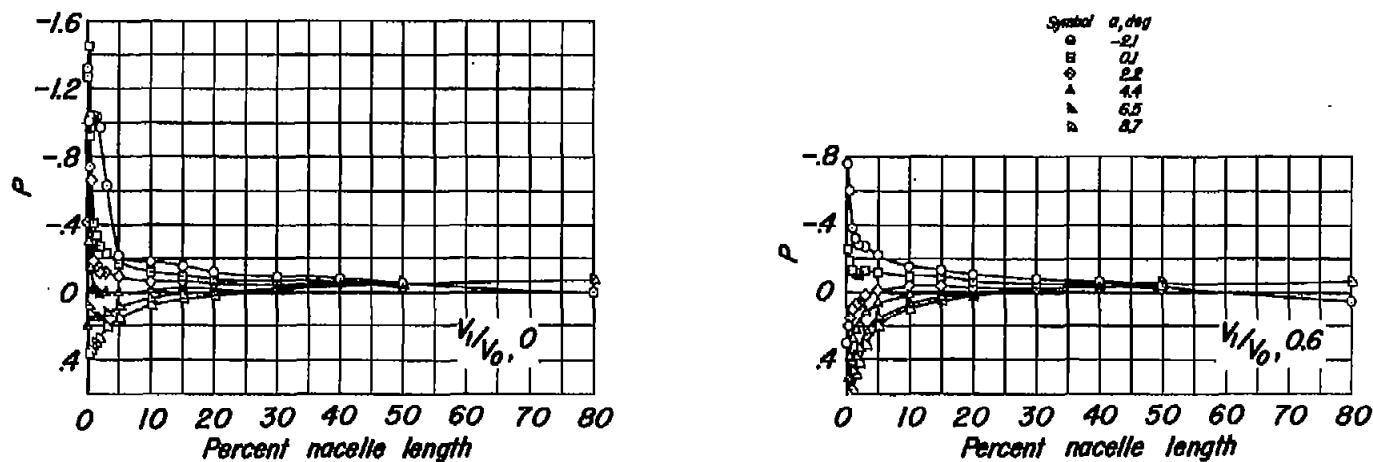


(c) Outboard lower wing-nacelle juncture.

Figure 21.—Pressure distribution for the nacelle in the understung inboard position with swept inlet.

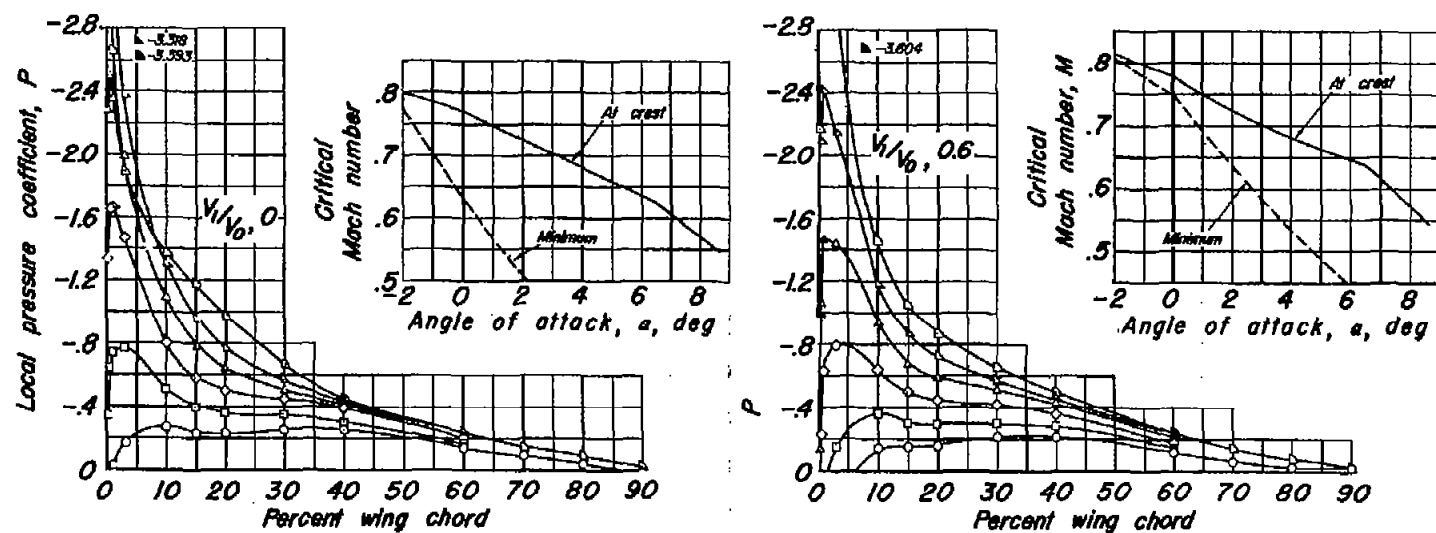


(a) Upper-surface center line:

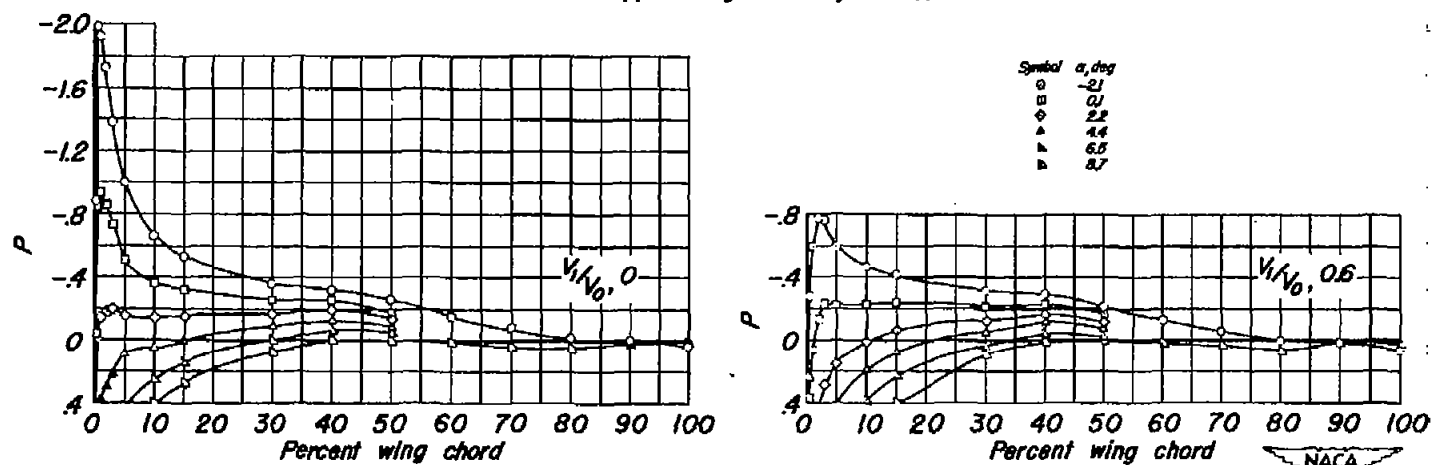


(b) Lower-surface center line.

Figure 22.- Pressure distribution and critical Mach number for the nacelle in the tip position.

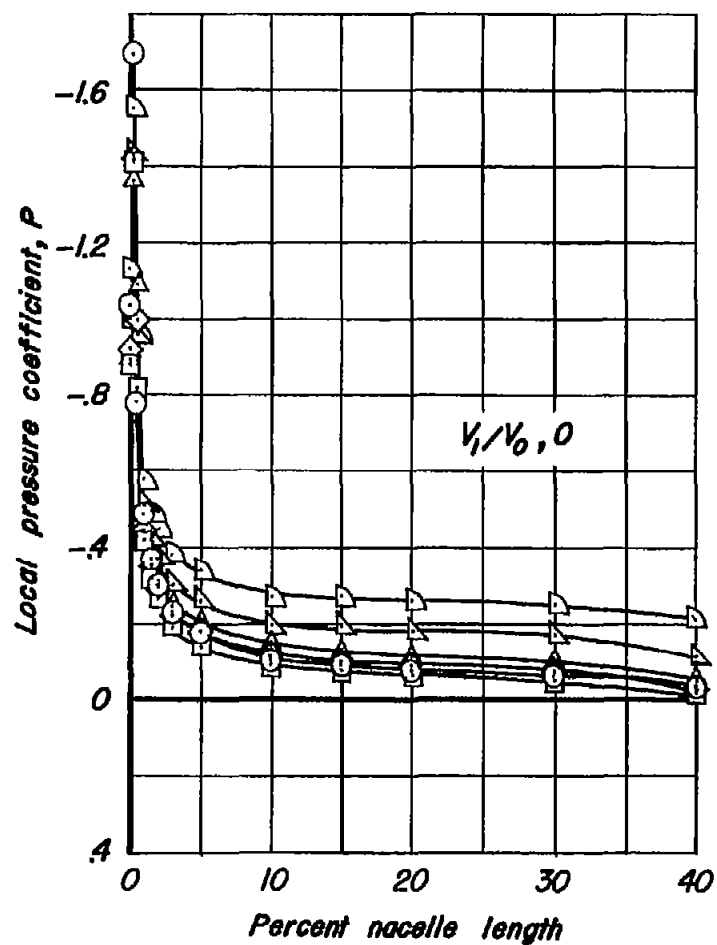


(c) Inboard upper wing-nacelle juncture.

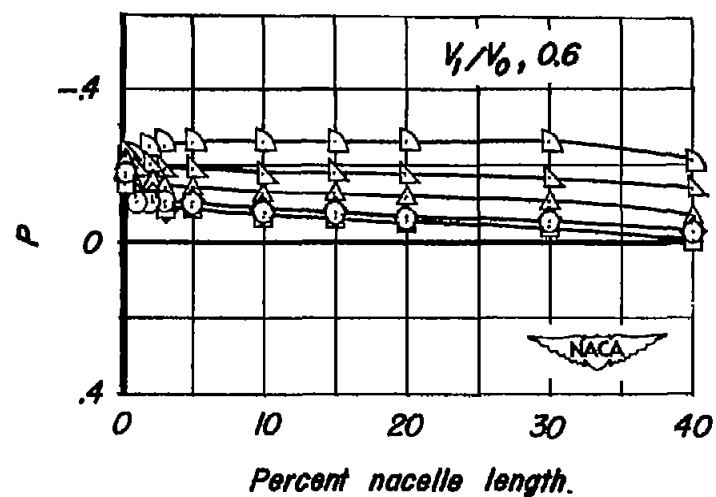


(d) Inboard lower wing-nacelle juncture.

Figure 22.—Continued.



Symbol	α, deg
○	-2.1
□	0.1
◇	2.2
△	4.4
▴	6.5
▷	8.7



(e) Outboard surface center line.

Figure 22.- Concluded.

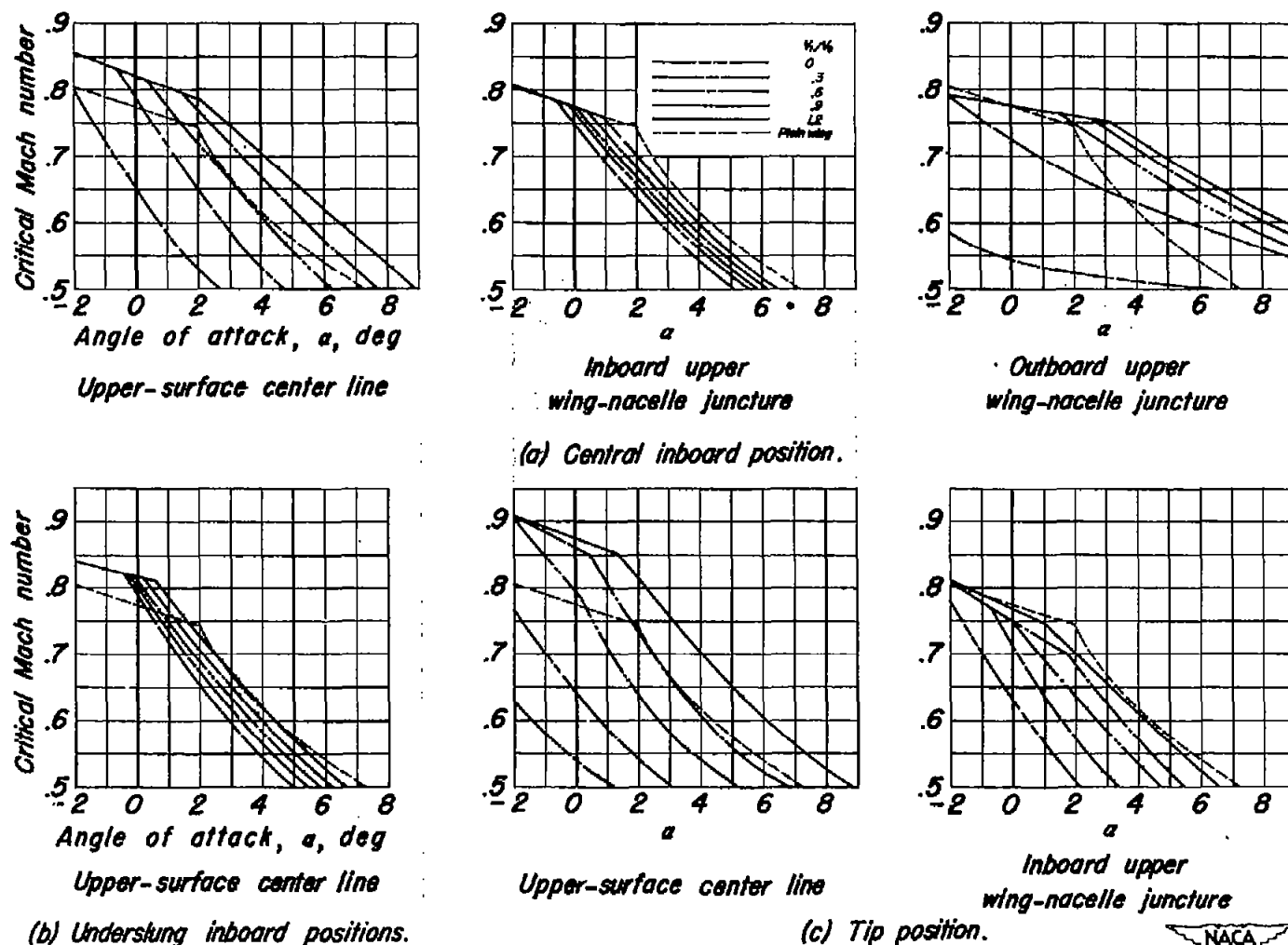
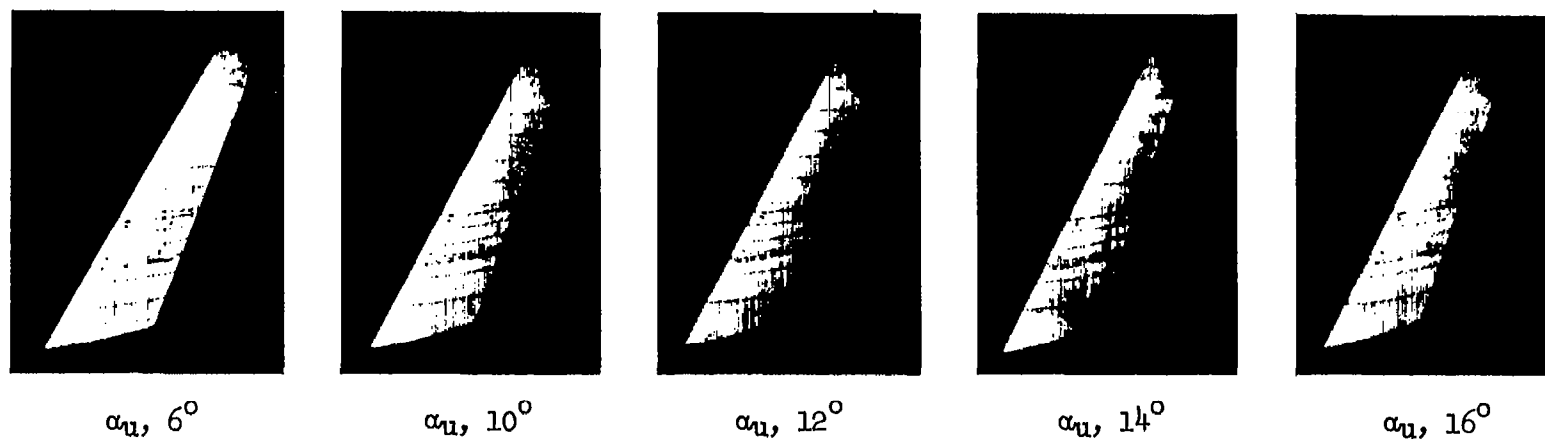
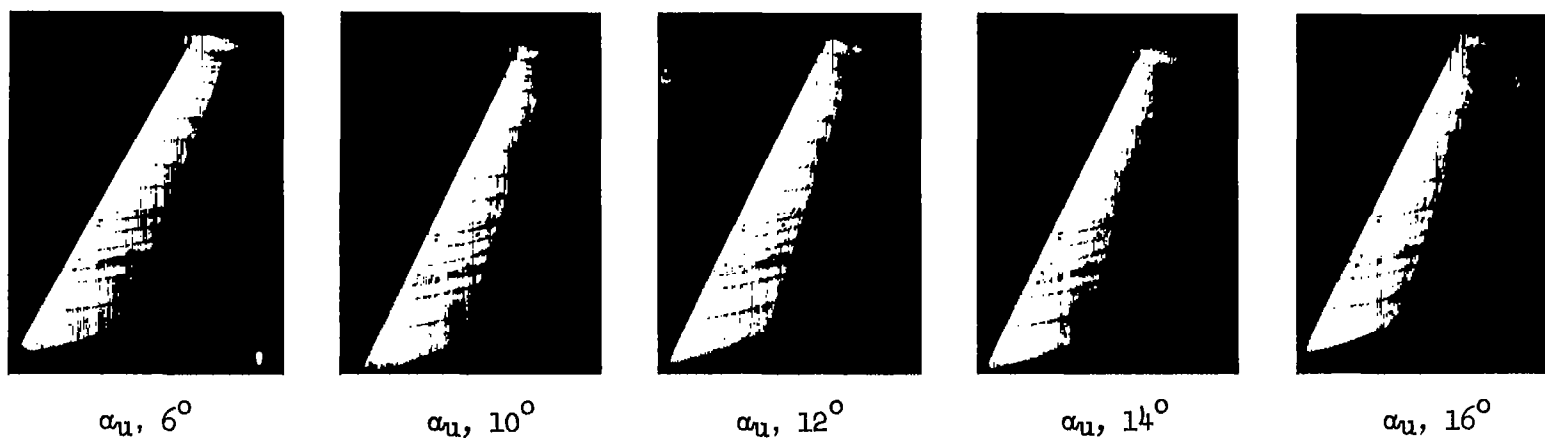


Figure 23.—Variation of the minimum critical Mach number for the nacelle in the various positions on the wing.



(a) Wing alone.



(b) Wing with nacelle in the tip position.

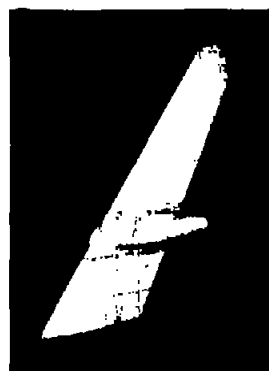
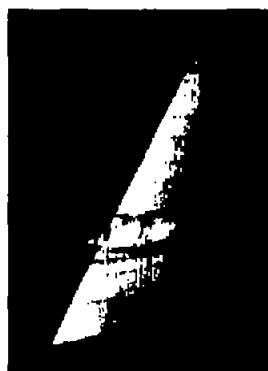
Figure 24.— Tuft studies over the upper surface of the wing and of the wing with nacelle.

•

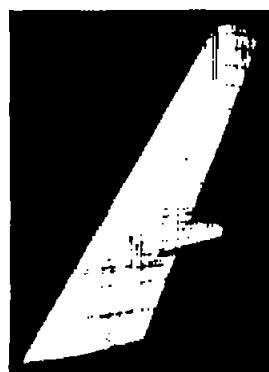
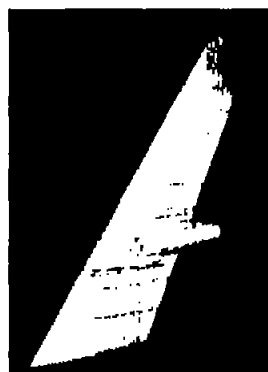
•

•

•

 $\alpha_u, 6^\circ$  $\alpha_u, 10^\circ$  $\alpha_u, 12^\circ$  $\alpha_u, 14^\circ$  $\alpha_u, 12^\circ$

(c) Wing with nacelle in the central inboard position.

 $\alpha_u, 6^\circ$  $\alpha_u, 10^\circ$  $\alpha_u, 12^\circ$  $\alpha_u, 14^\circ$  $\alpha_u, 16^\circ$

(d) Wing with nacelle in the underslung inboard position with normal inlet.



 A-12760

Figure 24.- Concluded.



3

1

2